Main Manuscript for

Prothoracicotropic hormone controls female sexual receptivity through the function of ecdysone in pC1 neurons of *Drosophila*

Jing Li[1,2,†,*], Chao Ning[3,†], Yaohua Liu[2,4,†], Bowen Deng[5], Bingcai Wang[2,6], Kai Shi[2,6], Rencong Wang[2,6], Ruixin Fang[1] and Chuan Zhou[1,2,6]

[1]*Institute of Molecular Physiology, Shenzhen Bay Laboratory, Shenzhen 518132, China*
[2]*State Key Laboratory of Integrated Management of Pest Insects and Rodents, Institute of Zoology, Chinese Academy of Sciences, Beijing 100101, China*
[3]*CAS Key Laboratory of Genome Sciences and Information, Beijing Institute of Genomics, Chinese Academy of Sciences, Beijing 100101, China*
[4]*Department of Plant Protection, Shanxi Agricultural University, Jinzhong 30801, China*
[5]*Chinese Institute for Brain Research, Peking-Tsinghua Center for Life Sciences, Zhongguancun Life Sciences Park, Beijing 102206, China*
[6]*University of Chinese Academy of Sciences, Beijing 100049, China*
[†]*These authors contributed equally to this work*

---

*Jing Li, Email: lijing@szbl.ac.cn

Author Contributions: Jing Li, Conceptualization, Resources, Data curation, Writing - original draft, review and editing, Funding acquisition; Chao Ning and Yaohua Liu, Data curation; Bowen Deng, Resources; Bingcai Wang, Kai Shi, Rencong Wang, Software; Ruixin Fang, Data curation; Chuan Zhou, Conceptualization, Funding acquisition.

Competing Interest Statement: The authors declare no competing interest.

Impact statement: Prothoracicotropic hormone and ecdysone belonging to the insect PG axis modulate virgin female sexual receptivity through regulating the morphological development of pC1b neurons.

Funding information: This work was supported by the Institute of Molecular Physiology, Shenzhen Bay Laboratory (NO.21260061 to Chuan Zhou, S239201006 to Jing Li), National Natural Science Foundation of China (NO.Y711241133 to Chuan Zhou) and Strategic Priority Research Program of the Chinese Academy of Sciences (NO.Y929731103 to Chuan Zhou).

Abstract

Female sexual receptivity is essential for reproduction of a species. Neuropeptides play the main role in regulating female receptivity. However, whether neuropeptides regulate the establishment of neural circuits for female sexual receptivity is unknown. Here we found the peptide hormone prothoracicotropic hormone (PTTH), which belongs to the insect PG axis, regulated virgin female receptivity through ecdysone during neural maturation in *Drosophila melanogaster*. We identified PG neurons expressing PTTH as doublesex-positive neurons, they regulated virgin female receptivity before the metamorphosis during the 3rd-instar larval stage. Furthermore, the ecdysone receptor EcR-A in pC1 neurons regulated virgin female receptivity during metamorphosis. The reduced EcR-A in pC1 neurons induced abnormal morphological development of pC1 neurons without changing neural activity. Among all subtypes of pC1 neurons, the function of EcR-A in pC1b neurons was necessary for virgin female copulation rate. These suggested that the changes of synaptic connections between pC1b and other neurons decreased female copulation rate. Moreover, analysis of brain transcriptomes when EcR-A was reduced in pC1 neurons revealed that, additional genes were regulated downstream of EcR-A function in pC1 neurons. The PG axis has similar functional strategy as the HPG axis in mammals to trigger the juvenile–adult transition. Our work suggests a general mechanism underlying which the neurodevelopment during maturation regulates female sexual receptivity.

Keywords: prothoracicotropic hormone, *Drosophila*, female sexual receptivity, ecdysone, pC1 neurons

Introduction

The success of copulation is important for the reproduction of a species. *Drosophila melanogaster* provides a powerful system to investigate the neuronal and molecular mechanism of sexual behaviors. Females decide to mate or not according to their physiological status and the environmental condition (Dickson, 2008). Sexually mature adult virgin females validate males after sensing the courtship song and male-specific sex pheromone, receive courtship with pausing and opening the vaginal plate (Ferveur, 2010; Greenspan et al., 2000; Hall, 1994; Wang et al., 2021). If female is not willing to mate, she may kick the legs, flick the wings, or extrude the ovipositor to deter males (Connolly et al., 1973). Mated females reject males for several days after mating mainly through more ovipositor extrusion and less opening the vaginal plate (Fuyama et al., 1997; Wang et al., 2021). These options need the establishment of neural circuits for female sexual receptivity. However, the associated mechanism of neural maturation and the effect of neural maturation on female sexual receptivity is little known.

doublesex (*dsx*) and *fruitless* (*fru*) are the terminal genes in sex determination regulatory hierarchy. They specify nearly all aspects of somatic sexual differentiation, including the preparation for sexual behaviors (Dickson, 2008; Manoli et al., 2013; Manoli et al., 2006; Mellert et al., 2012; Pavlou et al., 2013; Siwicki et al., 2009;

Yamamoto, 2007; Yamamoto et al., 2013). In males, male-specific *fru* protein (Fru^M) (Billeter et al., 2006; Demir et al., 2005; Hall, 1978; Manoli et al., 2005; Stockinger et al., 2005) and the male-specific *dsx* protein (Dsx^M) (Kohatsu et al., 2011; Pan et al., 2014; Pan et al., 2011; Rideout et al., 2010) are important for the male courtship behaviors. In females, functional Fru protein does not exist, while the neurons in that *fru* P1 promoter or *dsx* is expressed regulate some aspects of the female sexual behaviors (Kvitsiani et al., 2006; Rideout et al., 2010). *Fru and dsx* are involved in regulating the sexual dimorphism during neurodevelopment (Yamamoto et al., 2013). For instance, the sexual dimorphism of P1 and mAL neurons which are all associated with male courtship and aggression behaviors (Clowney et al., 2015; Hoopfer et al., 2015; Kimura et al., 2008; Kohatsu et al., 2011; Pan et al., 2012; Sengupta et al., 2022; von Philipsborn et al., 2011) is the result of regulation by Dsx and/or Fru (Ito et al., 2012; Kimura et al., 2008). In the cis-vaccenyl acetate (cVA) pathway, which induces the courtship inhibiting in males (Kurtovic et al., 2007; Wang et al., 2010), the first-order to the fourth-order components are all fruGAL4-positive neurons and are either male-specific or sexually dimorphic (Ruta et al., 2010). However, the role of Dsx^F in neurodevelopment associated with female sexual behaviors is little understood.

During postembryonic development, the PG axis triggers the juvenile–adult transition, similar as the function of hypothalamic–pituitary–gonadal (HPG) axis in mammals (Herbison, 2016; Pan et al., 2019). Hormones of the PG axis act to transform the larval nervous system into an adult version (Truman et al., 2023). Ecdysone belonging to the PG axis is the prime mover of insect molting and metamorphosis and is involved in all

112 phases of neurodevelopment, including neurogenesis, pruning, arbor outgrowth, and
113 cell death (Truman et al., 2023). The neurons read the ecdysteroid titer through two
114 isoforms of the ecdysone receptor, EcR-A and EcR-B1, according to spatial and
115 temporal conditions in the central nervous system (Riddiford et al., 2000; Truman et al.,
116 1994). EcR-A is required in fru P1-expressing neurons for the establishment of male-
117 specific neuronal architecture, and ecdysone receptor deficient males display increased
118 male–male courtship behavior (Dalton et al., 2009; Ganter et al., 2007). However, how
119 ecdysone regulates the neurodevelopment associated with female sexual receptivity,
120 especially the fru$^+$ and dsx$^+$ neurons, is unknown.
121
122 Much of studies to understand female sexual receptivity has focused on its regulation.
123 How a female respond to males is highly dependent on whether or not she has
124 previously mated. In virgin females, dsx$^+$ pCd neurons respond to the cVA, while dsx$^+$
125 pC1 neurons also respond to male courtship song (Zhou et al., 2014). The receptive
126 females open the vaginal plate (VPO) through activation of the dsx$^+$ vpoDN neurons
127 (Wang et al., 2021). After mated, sex peptide in the seminal fluid binds to the fru$^+$ dsx$^+$
128 sex peptide sensory neurons (SPSNs) in the female uterus. Then neuronal activity in
129 the dsx$^+$ sex peptide abdominal ganglion (SAG) neurons of the ventral nerve cord and in
130 the pC1 neurons is reduced (Avila et al., 2011; Feng et al., 2014; Häsemeyer et al.,
131 2009; Kubli, 2003; Wang et al., 2020b; Yang et al., 2009; Zhou et al., 2014). Therefore,
132 the sexual receptivity is reduced with less VPO and more ovipositor extrusion (OE)
133 which is controlled by dsx$^+$ DpN13 neurons (Wang et al., 2020a). In addition,
134 neuropeptides and monoamines play a critical role in regulation of the female

135 receptivity. The neuropeptides Drosulfakinin, myoinhibitory peptides and SIFamide are
136 involved in female sexual receptivity (Jang et al., 2017; Terhzaz et al., 2007; Wang et
137 al., 2022). As monoamines, dopamine, serotonin and octopamine are pivotal to female
138 sexual behaviors (Ishimoto et al., 2020; Ma et al., 2022; Neckameyer, 1998; Rezával et
139 al., 2014). So far, the identified neuropeptides and monoamines modulating female
140 sexual receptivity all function during the adult stage. However, whether neuropeptides
141 or monoamines regulate the establishment of neural circuits for female sexual
142 receptivity is unknown.
143
144 To explore the factors that regulate *Drosophila* virgin female receptivity especially
145 during neurodevelopment, we did a knock-out screen including most of CCT members.
146 We discovered a requirement for the prothoracicotropic hormone (PTTH) during
147 postembryonic development for virgin female receptivity. We also found that PG
148 neurons expressing PTTH are dsx^+ neurons. PTTH, a brain derived neuropeptide
149 hormone, is the primary promoter of the synthesis of steroid hormone 20-
150 hydroxyecdysone (20E) (McBrayer et al., 2007a; Rewitz et al., 2009). Indeed, the
151 enhanced virgin female receptivity due to the loss of PTTH could be rescued through
152 feeding 20E to the 3rd-instar larvae. Due to that 20E functions through its receptor EcR
153 (Riddiford et al., 2000), we then tested the function of EcR in pC1 neurons which
154 encode the mating status of females (Zhou et al., 2014). The reduced EcR-A expression
155 in pC1 neurons resulted in the unnormal anatomical pattern of pC1 neurons and the
156 reduced female copulation rate. Furthermore, the decreased female copulation rate was
157 due to the reduced EcR-A in pC1b neurons. To detect the molecular mechanism for the

158 regulation of pC1 neurons in virgin female receptivity, we tested the RNAseq when EcR-
159 A was reduced in pC1 neurons. We found some regulated genes, which provide clues
160 for our future research in the molecular mechanism by which pC1 neurons regulate
161 virgin female receptivity. Thus, in addition to demonstrating the function of PTTH in
162 virgin female receptivity during neural maturation, our study identified the necessary role
163 of the normal pC1b neural morphology in virgin female receptivity.
164
165 **Results**
166
167 **PTTH modulates virgin female receptivity**
168
169 In *Drosophila*, neuropeptides and monoamines, belonging to the chemoconnectome
170 (CCT) (Deng et al., 2019), play a critical role in regulation of the female receptivity. To
171 explore the factors that regulate virgin female receptivity especially during
172 neurodevelopment, we screened 108 chemoconnectome (CCT) knock-out lines
173 generated by the CRISPR-Cas9 system (Deng et al., 2019) (unpublished data). The
174 result showed that prothoracicotropic hormone (PTTH) might regulate virgin female
175 receptivity. The deletion mutant *⊿Ptth* removed part of the 5' UTR and almost all coding
176 sequence and is a protein null (**Figure 1A**). We confirmed the PTTH knock-out flies by
177 using PCR analysis at the PTTH locus in genomic DNA samples (**Figure 1B**), by using
178 RT-PCR to identify the loss of PTTH transcripts in cDNA samples (**Figure 1C**) and by
179 detecting the immunoreactivity of PTTH in the central brain (**Figure 1H**). Primers used
180 are listed in **Supplementary File 1**. PTTH immunoreactivity was found in the brain of

181 wild-type and heterozygous flies (**Figure 1 H1 and H3**), but was absent in homozygous
182 *ΔPtth* flies (**Figure 1H2**). As the previous study, the *ΔPtth* larvae lacking PTTH undergo
183 metamorphosis with about 1 day delay compared with the wild type control (Shimell et
184 al., 2018) (data not shown). Besides, the *ΔPtth* adult male and female flies had the
185 significant increased weight than wild type flies (**Figure 1—figure supplement 1A**).
186 This is also consistent with that PTTH regulates developmental timing and body size in
187 *Drosophila* (Mcbrayer et al., 2007b; Shimell et al., 2018).
188
189 To confirm the function of PTTH, we tested virgin female receptivity of *ΔPtth* female
190 flies. We found that the virgin female losing PTTH had significantly higher copulation
191 rate and shorter latency to copulation than wild type flies (**Figure 1 D-G**). In addition, the
192 *ΔPtth* flies had higher copulation rate and lower latency to copulation compared to
193 heterozygous null mutant females within 2 days (**Figure 1 D-E**) and within 3 days,
194 respectively (**Figure 1 D-F**). The enhanced virgin female receptivity had no relationship
195 either with the attractivity or with the locomotion activity of virgin females (**Figure 1—**
196 **figure supplement 1B-D**). These results suggested that PTTH participates in virgin
197 female receptivity in a dose-dependent manner.
198
199 Furthermore, we carried out genetic rescue experiments to further confirm the function
200 of PTTH in modulating virgin female receptivity. We used the pan-neuronal driver
201 elavGAL4 to drive UAS-PTTH expression in PTTH mutant background. We detected the
202 PTTH signals using PTTH antibody in the rescued female brains (**Figure 1H4**). We
203 found that neuron-specific expression of PTTH could restore the enhanced copulation

204 rate and shorter latency to copulation in *ΔPtth* virgin females (**Figure 1I**). These results
205 confirmed that PTTH modulates virgin female receptivity.
206
207 **Dsx$^+$ PG neurons regulate virgin female receptivity.**
208 We used new PtthGAL4 and PtthLexA which inserts GAL4 or LexA sequence before the
209 stop codon of the *Ptth* gene (Deng et al., 2019) to label and manipulate PG neurons
210 expressing PTTH. The labeled neurons were the same as reported before (McBrayer et
211 al., 2007a; Yamanaka et al., 2013), a pair of bilateral neurosecretory cells in the brain
212 directly innervating the prothoracic gland during the larval stage (**Figure 2A and Figure**
213 **2—figure supplement 1A**). The newly emerged flies had the similar anatomical pattern
214 with that of the larval stage (**Figure 2B and Figure 2—figure supplement 1B**).
215 However, while the prothoracic gland cells are gradually degenerating during pharate
216 adult development (Dai et al., 1991; Roy et al., 2018), the pattern of PG neurons labeled
217 by PtthGAL4 > UAS-mCD8GFP gradually could not be found before the 10th hour after
218 eclosion (**Figure 2—figure supplement 2**).
219
220 Most identified neurons associated with female sexual behaviors express *doublesex*
221 gene. We asked whether PG neurons are a part of the doublesex circuitry or not.
222 Double labeling of dsxLexA and PtthGAL4 neurons (LexAop-tomato,UAS-
223 stingerGFP/PtthLexA;dsxGAL4/+) revealed that PG neurons are all doublesex-positive
224 (**Figure 2C**). We then used an intersectional strategy to visualize overlapped expression
225 between dsxLexA and PtthGAL4 (UAS > stop > myrGFP/+;LexAop2-

226 FlpL,dsxLexA/PtthGAL4). We observed all PG neurons with GFP signals (**Figure 2D**).
227 These results suggested that PG neurons are dsx^+ neurons.
228
229 We then analyzed whether PG neurons are involved in the modulation of virgin female
230 receptivity. First, we activated PG neurons transiently in adult virgin females by driving
231 the temperature-sensitive activator dTrpA1 (Hamada et al., 2008) using PtthGAL4. PG
232 neurons were activated at 29°C compared with the control treatment at 23°C. No
233 significantly different copulation rate or latency to copulation was detected (**Figure 2—**
234 **figure supplement 3A-C**). This suggested that PG neurons do not regulate virgin
235 female receptivity during the adult stage.
236
237 To identify the detail time for the function of PG neurons in virgin female receptivity, we
238 inactivated PG neurons through kir2.1 under the control of the temporal and regional
239 gene expression targeting system (McGuire et al., 2004). The inactivation of PG
240 neurons during larval stage enhanced virgin female copulation rate significantly (**Figure**
241 **2E**). However, when PG neurons were inactivated during pupal or adult stages, virgin
242 female copulation rate did not change significantly (**Figure 2 F-G**). Furthermore, we
243 activated PG neurons at different stages overlapping the postembryonic larval
244 developmental time using dTrpA1 (**Figure 3A**). Stage 1 was from the 1st-instar larvae to
245 six hours before the 3rd-instar larvae. Stage 2 was from six hours before the 3rd-instar
246 larvae to the end of the wandering larvae. Stage 3 was from the end of wandering
247 larvae to the end of the 2nd day of the pupal stage. Stage 4 was from the end of the 2nd
248 day of the pupal stage to the eclosion of adults. The copulation rate did not change

249 significantly when activating PG neurons during the stage 1, stage 3 or stage 4 (**Figure**
250 **3B, 3D and 3E**). However, we found the significant lower copulation rate and the longer
251 latency to copulation only when PG neurons were activated during the stage 2 (**Figure**
252 **3C and Figure 3F**). The defected copulation was not due to a lower locomotion activity
253 of virgin females (**Figure 3G**). Taken together, our findings indicated that the activity of
254 dsx^+ PG neurons negatively regulate virgin female receptivity during the stage from the
255 start of the 3rd-instar to the end of wandering stage.
256
257 **PTTH modulates virgin female receptivity through ecdysone.**
258
259 The 3rd-intar larval stage is the critical stage for the initiation of metamorphosis involving
260 the synthesis of ecdysone (Imura et al., 2020; Lavrynenko et al., 2015; Shimell et al.,
261 2018). To test whether PTTH regulates virgin female receptivity through regulating the
262 synthesis of ecdysone, we rescued the enhanced female receptivity by feeding 20E to
263 the 3rd-intar larval *ΔPtth* flies. The enhanced copulation rate and shorter latency to
264 copulation of the *ΔPtth* flies were rescued to the comparable level of wild type females
265 (**Figure 4**). Furthermore, the wild type females fed by 20E had no significantly different
266 copulation rate and latency to copulation compared with the wild type females fed by the
267 same volume of 95% ethanol which is the solvent of 20E (**Figure 4**). This suggested
268 that PTTH regulates virgin female receptivity through the titer of ecdysone.
269
270 **Ecdysone receptor EcR-A in pC1 neurons regulates virgin female copulation rate.**
271

272 Given that PTTH regulates virgin female receptivity through ecdysone which acts on its
273 receptor EcR, we then asked that whether ecdysone regulates the function of neurons
274 associated with virgin female receptivity through EcR. pC1 and vpoDN neurons are two
275 main dsx^{+} neurons involved in virgin female receptivity (Wang et al., 2021; Zhou et al.,
276 2014). pC1 neurons encode the mating status of female flies, vpoDN neurons regulate
277 the opening of vaginal plate when females attend to accept males. EcR-A and EcR-B1
278 are the two prominently expressed ecdysone receptors in the CNS (Riddiford et al.,
279 2000). First, we tested the expression of EcR-A and EcR-B1 in these two neurons on
280 the 2nd day of the pupal stage when ecdysone functions as the main mover in the
281 metamorphosis (Dalton et al., 2009; Truman et al., 1994). The GFP signals labeled by
282 pC1-ss2-GAL4 and vpoDN-ss1-GAL4 were merged well with the signals of both EcR-A
283 and EcR-B1 antibodies respectively (**Figure 5—figure supplement 1**). This revealed
284 that EcR-A and EcR-B1 express in both pC1 and vpoDN neurons. We then tested the
285 function of EcR in pC1 and vpoDN neurons through reducing the expression of EcR-A
286 and EcR-B1 respectively. We used the split GAL4 for pC1 and vpoDN neurons to drive
287 the UAS-EcR-RNAi. First, we reduced the expression of all EcR isoforms in pC1
288 neurons, this decreased the copulation rate and prolonged the latency to copulation
289 significantly (**Figure 5—figure supplement 2A**). Furthermore, we reduced the
290 expression of EcR-A in pC1 neurons. The virgin female had the significant lower
291 copulation rate and longer latency to copulation (**Figure 5A**). The reduced copulation
292 rate had no relationship with the attractivity (**Figure 5E**) and the locomotion activity of
293 virgin females (**Figure 5—figure supplement 2B**). When reducing the expression of
294 EcR-B1 in pC1 neurons, virgin females had the significant longer latency to copulation

295 but the comparable copulation rate to controls (**Figure 5B**). However, reducing the
296 expression of EcR-A (**Figure 5—figure supplement 3 A-C**) and EcR-B1 (**Figure 5—**
297 **figure supplement 3 D-F**) using three split vpoDNGAL4s in vpoDN neurons all did not
298 affect virgin female receptivity. This suggested that the expression of EcR-A in pC1
299 neurons regulates virgin female copulation rate, but EcR isoforms in vpoDN neurons do
300 not modulate virgin female receptivity.
301
302 Two split-GAL4 drivers for pC1 neurons had been obtained previously. pC1-ss1-GAL4
303 labels pC1-a, c and -e neurons, and pC1-ss2-GAL4 labels all pC1-a, -b, -c, -d and -e
304 neurons (Wang et al., 2020b). We also tested virgin female receptivity when EcR-A or
305 EcR-B1 were reduced in pC1-a, -c and -e neurons simultaneously using pC1-ss1-GAL4
306 respectively. While the copulation rate or the latency to copulation did not change
307 significantly (**Figure 5 C-D**). This suggested that, pC1b and/or pC1d neurons are
308 necessary for the functions of EcR-A and EcR-B1 in pC1 neurons on virgin female
309 receptivity. Whether pC1d is involved in the regulation of female receptivity is uncertain
310 (Deutsch et al., 2020; Schretter et al., 2020; Taisz et al., 2023). However, when
311 reducing EcR-A in pC1d neurons alone using the specific split GAL4 SS56987
312 (Schretter et al., 2020), virgin female receptivity including copulation rate and latency to
313 copulation did not change significantly compared with controls (**Figure 5—figure**
314 **supplement 4**). These results suggested that the function of EcR-A in pC1b neurons is
315 necessary for virgin female copulation rate.
316

317 As recently mated females may reduce sexual receptivity and increase egg laying (Avila
318 et al., 2011; Kubli, 2003). we asked whether the decreased copulation rate induced by
319 EcR-A could be a post-mating response and correlate with elevated egg laying. To
320 address this, we examined the number of eggs laid by virgin females when EcR-A was
321 reduced in pC1 neurons. We found that manipulation of EcR-A did not enhance egg
322 laying significantly in virgin females (**Figure 5F**). Meanwhile, we further analyzed
323 whether reduction of EcR-A in pC1 neurons regulates the opening of vaginal plate
324 (VPO) or the ovipositor extrusion (OE). We found that reducing the EcR-A expression in
325 pC1 neurons lead to the significantly less VPO and more OE (**Figure 5 G-H**). These
326 results suggested that reduced EcR-A expression in pC1 neurons results in the similar
327 phenotype to that of mated females.
328
329 **EcR-A participates in the morphological development of pC1 neurons.**
330
331 EcR isoforms have distinct temporal and spatial expression patterns in the CNS
332 (Riddiford et al., 2000; Truman et al., 1994). It is unknown when EcR-A functions in pC1
333 neurons for virgin female receptivity. Thus, we examined virgin female receptivity when
334 EcR-A expression was conditionally reduced through RNAi via the pC1-ss2-GAL4 under
335 the control of the temporal and regional gene expression targeting system (McGuire et
336 al., 2004). EcR-A was reduced during the larval, pupal and adult stage respectively
337 (**Figure 5 I-K**). Only during the pupal stage, reducing EcR-A made the significant lower
338 copulation rate and longer latency to copulation (**Figure 5J**). The result suggested that
339 EcR-A in pC1 neurons plays a role in virgin female receptivity during metamorphosis.

340 This is consistent with that PTTH regulates virgin female receptivity before the start of
341 metamorphosis which is around the puparium formation.
342
343 We then tested how EcR-A functions in pC1 neurons to modulate virgin female
344 receptivity. First, we tested the morphology of pC1 neurons when reducing the
345 expression of EcR-A in pC1 neurons. We found that the morphology of pC1 neurons
346 appeared after the formation of the white pupa (Figure **6A1**). The reduced EcR-A
347 expression induced the more elaborated morphologies of the pC1-d/e cells, especially
348 the extra vertical projection (EVP) near the midline of brains (**Figure 6 B-D**) (Deutsch et
349 al., 2020). These changes exhibited from the second day of the pupal stage (**Figure 6**
350 **B1-B2 and 6E**) and maintained at the adult stage (**Figure 6 D1-D2 and 6F**). Meanwhile,
351 the number of pC1 cell bodies in adult flies when EcR-A was reduced were the same as
352 that of wild type flies (**Figure 6G**). Previous studies suggested that pC1d cells serve as
353 a hub within the central brain for dsx^+ and fru^+ neurons (Deutsch et al., 2020). Thus, the
354 unnormal development of pC1d neurons may induce the changes between pC1d
355 neurons and other dsx^+ and fru^+ neurons to affect associated behaviors.
356
357 Furthermore, we asked whether reduced female copulation rate was due to that EcR-A
358 expression affected the activity of pC1 neurons. Because all pC1 cells characterized so
359 far project to the lateral junction of the lateral protocerebral complex (LPC) (Kimura et
360 al., 2015; Rezával et al., 2016; Scheffer et al., 2020; Wang et al., 2020b; Wu et al.,
361 2019; Zhou et al., 2014), we expressed GCamp6s in all pC1 neurons and tested the
362 calcium signals in the lateral junction of LPC when EcR-A was knocked down (**Figure 6**

363 **D1-D2**). Reduced EcR-A did not induce significantly different calcium responses in the
364 LPC (**Figure 6H**). Thus, our results suggested that the decreased female copulation
365 rate induced by reduced EcR-A in pC1 neurons was mainly due to the morphological
366 changes of pC1b neurons, which then modulate the connections of pC1b neurons with
367 other neurons.
368
369 **Reduction of EcR-A in pC1 neurons affects gene expression.**
370
371 To further detect the factors that were regulated downstream of EcR-A in pC1 neurons
372 for the function in virgin female receptivity, we tested the transcriptome of brain in adult
373 virgin females when EcR-A was knocked down in pC1 neurons. We focused on the
374 differently expressed genes of the 4th day after eclosion when mating behaviors were
375 tested. We identified 527 differentially expressed ($p < 0.01$) genes, 123 of which passed
376 a false discovery rate (FDR) cutoff of 0.01 (**Figure 7, Supplementary File 2 and**
377 **Supplementary File 3**).
378
379 The gene encoding dopamine beta-monooxygenase (DBM) was the top most down-
380 regulated gene (**Figure 7 A-B**). The mammal homolog of DBM is monooxygenase
381 DBH-like 1 (Moxd1). Moxd1 has the similar structure as the mammal dopamine β-
382 hydroxylase (DBH) which is the enzyme for transition from dopamine to norepinephrine
383 (Park et al., 1976; Prigge et al., 2000; Vendelboe et al., 2016). This implied that DBM is
384 probably related to the dopamine metabolism. It will be interesting to study the function
385 of DBM in virgin female receptivity. Besides, CG30428 protein was also down-regulated

386 (**Supplementary File 2)**. It is predicted to be active in nucleus, suggesting its role in
387 gene expression and cellular metabolism. This is consistent with that reduction of EcR-
388 A in pC1 neurons induced the unnormal anatomical morphology of pC1 neurons, which
389 may due to the unnormal cell death and cellular differentiation during development.
390

391 **Discussion**

392

393 In this study, we found that peptide hormone PTTH modulates virgin female receptivity
394 through ecdysone during neural maturation. PG neurons expressing PTTH are
395 doublesex-positive and regulate virgin female receptivity during the 3rd-instar larval
396 stage. Furthermore, ecdysone receptor EcR-A functions in pC1 neurons to regulate
397 virgin female copulation rate during the metamorphosis mainly through modulating the
398 anatomical morphology of pC1b neurons. Taken together, our results identified the
399 function of PTTH-ecdysone and their downstream pathway, EcR-A in pC1 neurons, on
400 regulating virgin female copulation rate during neural maturation mainly through
401 modulating the morphology of pC1b neurons.
402

403 Our results suggested a regulatory role of PTTH in virgin female receptivity. Even
404 though insects and mammals represent highly diverged classes, insects have evolved a
405 similar strategy for triggering the juvenile–adult transition (Herbison, 2016; Pan et al.,
406 2019). The juvenile–adult transition involves the hypothalamic–pituitary–gonadal (HPG)
407 axis in mammals and the PG axis in insects. Among the neurons belonging to the axis,
408 PG neurons and GnRH neurons have the similar function to stimulate the PG gland and

409 pituitary gland to release hormones which trigger maturation, respectively. It will be
410 interesting to study the function of GnRH neurons in the mammal sexual behaviors.
411 Most of neurons regulating sexual behaviors in female flies are dsx$^+$ neurons. Our
412 results showed that PG neurons are also dsx$^+$ neurons. This suggested that PG
413 neurons have relationships with other dsx$^+$ neurons and the juvenile–adult transition is
414 regulated by *doublesex* gene.
415
416 In our study, PTTH regulates virgin female receptivity in an ecdysone-dependent
417 manner before the peak of ecdysone for the metamorphosis. Ecdysone functions
418 through its receptor EcR which is involved in all phases of the nervous system
419 development. Previous studies have demonstrated that the fru$^+$ neuron development
420 need EcR-A in male *Drosophila melanogaster*. Furthermore, reduced EcR-A in fru$^+$
421 neurons induced the male-male courtship (Dalton et al., 2009). In females, we detected
422 the expression of EcR-A and EcR-B1 in both dsx$^+$ pC1 and dsx$^+$ vpoDN neurons.
423 However, EcR regulates virgin female receptivity in pC1 neurons but not in vpoDN
424 neurons. This may due to that EcR does not regulate the morphology of vpoDN neurons
425 and thus the synaptic connections with other neurons. Alternatively, EcR regulates the
426 morphology of vpoDN neurons without changing functional connectivity or gene
427 expressions within associated neurons. It is worth noting that the losing of PTTH
428 resulted in the enhanced virgin female receptivity, which is contrary to the reduced
429 receptivity when knocking down EcR-A in pC1 neurons. This may due to that 20E and
430 EcR regulates multiple neurodevelopment associated with virgin female receptivity

431 when PTTH is knocked out, but not only functions in pC1 neurons. This may also due to
432 that PTTH mutant results in increased EcR expression in pC1 neurons.
433
434 Reduced EcR-A expression in all pC1 neurons lead to the decreased copulation rate,
435 while reduced EcR-A in pC1-a, c and e simultaneously did not reduce the copulation
436 rate significantly. This suggested that EcR-A plays the critical role in pC1-b or/and -d
437 neurons for regulating virgin female receptivity. Our results revealed that reduced EcR-
438 A induced the more elaborated morphologies of pC1d neurons. Previous studies
439 detected the synaptic connections between the axons of pC1d and the dendrites of
440 DNp13 neurons (Deutsch et al., 2020; Mezzera et al., 2020). DNp13 neurons are
441 command neurons for ovipositor extrusion. When females extruded, the ovipositor
442 physically impedes copulation (Mezzera et al., 2020; Wang et al., 2020a). However,
443 reduced EcR-A expression in pC1d neurons did not affect virgin female receptivity
444 (**Figure 5—figure supplement 4**). This might be due to three possibilities. First, the
445 more elaborated morphologies of pC1d neurons did not affect synaptic connections
446 between pC1d and DNp13 neurons. Second, the unchanged pC1 neural activity could
447 not affect the neural activity of DNp13 neurons. Third, the morphological change of
448 pC1d neurons is not sufficient for the decreased copulation rate. To sum, these suggest
449 that the morphological change of pC1b neurons is necessary for the decreased
450 copulation rate. However, due to the lack of pC1b drivers, we could not rule out
451 morphological changes in pC1b neurons when EcR-A was reduced.
452

453 We identified DBM as the mostly down-regulated gene when EcR-A was reduced in
454 pC1 neurons. DBM is the insect homolog of MOXd1 in mammals. However, the function
455 of MOXd1 has not been identified but is predicted to hydroxylate a hydrophobic
456 substrate (Xin et al., 2004). The similar structure between MOXd1 and dopamine beta-
457 monooxygenase in mammals suggests the possible role of DBM in dopamine
458 metabolism (Cubells et al., 2004; Kim et al., 2002; Timmers et al., 2004). Besides,
459 previous study identified the Moxd1 as a useful marker for the sexually dimorphic nuclei
460 and may be involved in the regulation of sex-biased physiology and behaviors in
461 mammals (Tsuneoka et al., 2017). These make it interesting to further study on the
462 molecular mechanism by which DBM and Moxd1 regulate sexual behaviors in flies and
463 mammals respectively.
464
465 Taken together, this study demonstrates that the peptide hormone PTTH, expresses in
466 dsx^+ PG neurons, regulates virgin female receptivity during neural maturation. It also
467 revealed that the morphological development of pC1b neurons regulated by EcR-A is
468 necessary for virgin female copulation rate. This work extends the understanding of how
469 neurodevelopmental processes regulate adult sexual behavior.
470
471 **Materials and methods**
472
473
474
475

Key Resources Table				
Reagent type (species) or resource	**Designation**	**Source or reference**	**Identifiers**	**Additional information**
antibody	Mouse anti-Bruchpilot antibody (nc82)	Developmental Studies Hybridoma Bank	Cat# nc82, RRID: AB_2314866	IHC (1:40)
antibody	Mouse Anti-Drosophila ecdysone receptor (EcR-A) Monoclonal Antibody	Developmental Studies Hybridoma Bank	Cat# 15G1a (EcR-A), RRID: AB_528214	IHC (1:10)
antibody	mouse Anti-Drosophila ecdysone receptor (EcR-B1) Antibody	Developmental Studies Hybridoma Bank	Cat# AD4.4(EcR-B1), RRID: AB_2154902	IHC (1:10)
antibody	Rabbit polyclonal anti-GFP	Thermo Fisher Scientific	Cat# A-11122, RRID: AB_221569	IHC (1:1000)
antibody	chicken polyclonal anti-GFP	Thermo Fisher Scientific	Cat# A10262, RRID: AB_2534023	IHC (1:1000)
antibody	Goat anti-rabbit, Alexa Fluor 488	Thermo Fisher Scientific	Cat# A-11034, RRID: AB_2576217	IHC (1:500)
antibody	Goat anti-chickent, Alexa Fluor 488	Thermo Fisher Scientific	Cat#A-11039; RRID: AB_2534096	IHC (1:500)
antibody	Goat anti-mouse, Alexa Fluor 488	Thermo Fisher Scientific	Cat# A-11029, RRID: AB_2534088	IHC (1:500)
antibody	Goat anti-rabbit, Alexa Fluor 546	Thermo Fisher Scientific	Cat# A-11010, RRID: AB_2534077	IHC (1:500)
antibody	Rabbit polyclonal anti-RFP	Thermo Fisher Scientific	Cat# R10367, RRID: AB_10563941	IHC (1:500)
antibody	Goat anti-mouse, Alexa Fluor 647	Thermo Fisher Scientific	Cat# A-21235, RRID: AB_2535804	IHC (1:500)
antibody	Rabbit polyclonal anti-PTTH	Zhou Lab, Chinese Academy of Sciences, this paper	N/A	IHC (1:1300)
chemical compound, drug	Paraformaldehyde (PFA)	Electron Microscopy Sciences	Cat#15713	8% PFA diluted in 1XPBS at 1:4 or 1:2
chemical compound, drug	DPX Mountant	Sigma-Aldrich	Cat#44581	
chemical compound, drug	Normal goat serum	Sigma-Aldrich	Cat#G9023	
chemical compound, drug	20-hydroxyecdysone	Cayman	Cat#16145	dissolved in 95% ethanol, 0.2 mg/ml
chemical compound, drug	TRIzol	Ambion	Cat#15596018	
Genetic reagent (*D.melanogaster)*	*LexAop2-mCD8::GFP*	Bloomington Stock Center	BL#32203	
Genetic reagent (*D.melanogaster)*	*;;UAS-mCD8::GFP*	Bloomington Stock Center	BL#32194	
Genetic reagent (*D.melanogaster)*	*;UAS-mCD8::GFP;*	Bloomington Stock Center	BL#5137	
Genetic reagent (*D.melanogaster)*	*UAS-dTrpA1/cyo*	Garrity Lab, Brandeis University	N/A	
Genetic reagent (*D.melanogaster)*	*UAS-Kir2.1*	Bloomington Stock Center	BL#6595	

Genetic reagent (*D.melanogaster)*	*PtthGAL4*	Rao Lab, Peking University	N/A	
Genetic reagent (*D.melanogaster)*	*PtthLexA*	Rao Lab, Peking University	N/A	
Genetic reagent (*D.melanogaster)*	*ΔPTTH*	Rao Lab, Peking University	N/A	
Genetic reagent (*D.melanogaster)*	*UAS-PTTH*	Zhou Lab, Chinese Academy of Sciences, this paper	N/A	
Genetic reagent (*D.melanogaster)*	*isoCS*	Rao Lab, Peking University	N/A	
Genetic reagent (*D.melanogaster)*	*elav-GAL4*	Rao Lab, Peking University	N/A	
Genetic reagent (*D.melanogaster)*	*UAS-GFPStinger*	Janelia Research Campus	N/A	
Genetic reagent (*D.melanogaster)*	*LexAop-tomato*	Janelia Research Campus	N/A	
Genetic reagent (*D.melanogaster)*	*LexAop2-FlpL*	Janelia Research Campus	N/A	
Genetic reagent (*D.melanogaster)*	*UAS > stop > mCD8-GFP*	Janelia Research Campus	N/A	
Genetic reagent (*D.melanogaster)*	*dsxGAL4*	Janelia Research Campus	N/A	
Genetic reagent (*D.melanogaster)*	*dsxLexA*	Janelia Research Campus	N/A	
Genetic reagent (*D.melanogaster)*	*tub-GAL80^{ts}*	Pan Lab, Southeast University	BL#7018	
Genetic reagent (*D.melanogaster)*	*pC1-ss1-GAL4*	Wang Lab, Lingang Laboratory	N/A	
Genetic reagent (*D.melanogaster)*	*pC1-ss2 GAL4*	Wang Lab, Lingang Laboratory	N/A	
Genetic reagent (*D.melanogaster)*	*vpoDN-ss1-GAL4*	Wang Lab, Lingang Laboratory	N/A	
Genetic reagent (*D.melanogaster)*	*vpoDN-ss2-GAL4*	Wang Lab, Lingang Laboratory	N/A	
Genetic reagent (*D.melanogaster)*	*vpoDN-ss3-GAL4*	Wang Lab, Lingang Laboratory	N/A	
Genetic reagent (*D.melanogaster)*	*UAS-EcR-RNAi*	Bloomington Stock Center	BL#9327	
Genetic reagent (*D.melanogaster)*	*UAS-EcR-A-RNAi*	Bloomington Stock Center	BL#9328	
Genetic reagent (*D.melanogaster)*	*UAS-EcR-B1-RNAi*	Bloomington Stock Center	BL#9329	
Genetic reagent (*D.melanogaster)*	*pC1d-GAL4*	Bloomington Stock Center	BL#86847	
recombinant DNA reagent	pBSK-attP-3P3-RFP-loxP	Bowen Deng et al., 2019	N/A	

recombinant DNA reagent	pBSK-attB-loxP-myc-T2A-Gal4-GMR-miniwhite	Bowen Deng et al., 2019	N/A	
recombinant DNA reagent	pBSK-attB-loxP-V5-T2A-LexA::p65-GMR-miniwhite	Bowen Deng et al., 2019	N/A	
software, algorithm	MATLAB	MathWorks, Natick, MA	https://www.mathworks.com/products/matlab.html	
software, algorithm	ImageJ	National Institutes of Health	https://imagej.nih.gov/ij/	
software, algorithm	Prism 7	GraphPad	https://www.graphpad.com/	
software, algorithm	R 4.1.3	RStudio	https://www.r-project.org	

Fly stocks

Flies were reared on standard cornmeal-yeast medium under a 12 hr:12 hr dark:light cycle at 25°C and 60% humidity. All the knock-out lines in this study for screening have been published [49]. The following strains were obtained from Dr. Yi Rao: *isoCS* (wild-type), *ΔPtth*, *PtthGAL4, PtthLexA, elavGAL4 and UAS-Kir2.1* (BL#6595). UAS-dTrpA1 was a gift from Dr. Paul Garrity. *UAS-GFPStinger*, *LexAop-tomato, LexAop2-FlpL, UAS > stop > mCD8-GFP*, *dsxGAL4* and *dsxLexA* (Mellert et al., 2010) have been described previously (Pfeiffer et al., 2008; Pfeiffer et al., 2010) and are obtained from Janelia Research Campus. *tub-GAL80^{ts}* (BL#7018) was provided by Dr. Yufeng Pan. *pC1-ss1-GAL4, pC1-ss2 GAL4, vpoDN-ss1-GAL4, vpoDN-ss2-GAL4* and *vpoDN-ss3-GAL4* were provided by Dr. Kaiyu Wang. The following lines were obtained from the Bloomington Drosophila Stock Center: *UAS-EcR-RNAi* (BL#9327), *UAS-EcR-A-RNAi* (BL#9328), *UAS-EcR-B1-RNAi* (BL#9329), *UAS-mCD8::GFP* (BL#32194), *LexAop2-mCD8::GFP* (BL#32203), *UAS-mCD8::GFP* (BL#5137) and *pC1d-GAL4* (BL#86847).

Behavioral assays

494

495 Flies were reared at 25°C and 60% humidity under a 12 hr light:12 hr dark cycle. Virgin
496 females and wild-type males were collected upon eclosion, placed in groups of 12 flies
497 each and aged 4–6 days (except for the assays for PTTH mutant on different days after
498 eclosion, and the molecular rescue assay for the 24h-old females) before carrying out
499 behavioral assay except for the transient thermogenetic experiments. Female receptivity
500 assays were conducted as previously described (Wang et al., 2022; Zhou et al., 2014).
501 A virgin female of defined genotype and a wild type male were gently cold anesthetized
502 and respectively introduced into two layers of the courtship chambers separated by a
503 removable transparent film. The flies were allowed to recover for at least 45 min before
504 the film was removed to allow the pair of flies to contact. The mating behavior was
505 recorded using a camera (Canon VIXIA HF R500) for 30 min at 17 fps for further
506 analysis.

507

508 For transient activation experiment by dTrpA1 in adult stage, flies were reared at 23°C.
509 Flies were loaded into courtship chamber and recovered for at least 30 min at 23°C,
510 then were placed at 23°C (control group) or 29°C (experimental group) for 30 min prior
511 to removing the film and videotaping. For activation experiment by dTrpA1 during
512 development, flies were reared at 29°C during the specific stages compared with the
513 controls who were reared at 23°C all the time. Flies were loaded into courtship chamber
514 and recovered for at least 45 min at 23°C prior to removing the film and videotaping.

515

516 **Quantification and statistical analysis of female receptivity behavior**

517

518 Two parameters including copulation rate and latency to copulation were used to
519 characterize receptivity and we got the data sets of two parameters from the same flies.
520 The time from removing the film to successful copulation was measured for each
521 female. The number of females that had engaged in copulation by the end of each 1
522 min interval within 30 min were summed and plotted as a percentage of successful
523 copulation. The latency to copulation was the time from removing the film to successful
524 copulation. All the time points that female successfully copulated were manually
525 analyzed and the data of unhealthy flies were discarded.

526

527 **Temporally restricted RNAi**

528

529 tub-GAL80^{ts} crosses were reared at either 18°C for control groups or 30°C for
530 experimental groups. Virgin females were collected at eclosion and were placed in
531 groups of 12 flies each and aged 4–6 days before carrying out behavior assay. Assays
532 were tested at 23°C.

533

534 **Male courtship index**

535

536 Courtship index was defined as the proportion of time the male followed, oriented
537 toward and attempted to copulate the female within 5 min of courtship initiation, marked
538 by the initial orientation toward and following the female.

539

540 **Vaginal plate opening and ovipositor extrusion**

541

542 A virgin female of defined genotype and a wild type male were aspirated into the
543 courtship chambers and respectively introduced into two layers of the courtship
544 chambers separated by a removable transparent film. The flies were allowed to recover
545 for 30 min before the film was removed. To allow visualization of vaginal plate opening,
546 we recorded uncompressed image sequences at 896 x 896 pixels and 50 frames per
547 second using a Photron Mini AX camera (Photron) with an AF-S VR Micro-Nikkor
548 105mm lens (Nikon). Instances of vaginal plate opening and ovipositor extrusion were
549 scored blind to genotype from frame by-frame playback during the first 5 min of
550 courtship or until copulation if it occurred within 5 min. Courtship initiation was defined
551 as the male orienting toward and beginning to follow the female. Rare trials with fewer
552 than 30 s of total courtship were discarded.

553

554 **Locomotion assays**

555

556 The rearing and experimental conditions in locomotion assays were the same as that in
557 the corresponding female receptivity assays, excepting that individual females were
558 loaded in the chambers without males. Spontaneous movements of the flies were
559 recorded with a camera (Canon VIXIA HF R500) for 30 min at 30 fps for further
560 analysis. The activity of flies during the middle 10 min was analyzed to calculate the
561 average walking speed using Ctrax software.

562

563 **Egg Laying**

564

565 Virgin females were collected upon eclosion and one fly was housed on standard
566 medium at 25°C, 60% relative humidity, 12 hr light:12 hr dark and allowed to lay eggs in
567 single vials. Each fly was transferred into new food tube every 24 hr. The number of
568 eggs was counted at the end of each 24 hr period. The numbers during the 3rd and 4th
569 day were summed for statistics and plot.

570

571 **Immunohistochemistry**

572

573 Whole brains of flies were dissected in 1x PBS and fixed in 2% paraformaldehyde
574 diluted in 1x PBS for 55 min at room temperature. The samples were washed with PBT
575 (1x PBS containing 0.3% Triton X-100) for 1 hour (3 x 20 min), followed by blocking in
576 5% normal goat serum (Blocking solution, diluted in 0.3% PBT) for 1 hour at room
577 temperature. Then, the samples were incubated in primary antibodies (diluted in
578 blocking solution) for 18–24 hours at 4°C. Samples were washed with 0.3% PBT for 1
579 hour (3 x 20 min), then were incubated in secondary antibodies (diluted in blocking
580 solution) for 18–24 hours at 4°C. Samples were washed with 0.3% PBT for 1 hour (3 x
581 20 min), then were fixed in 4% paraformaldehyde for 4 hours at room temperature. After
582 washed with 0.3% PBT for 1 hour (3 x 20 min), brains were mounted on poly-L-lysine-
583 coated coverslip in 1x PBS. The coverslip was dipped for 5 min with ethanol of
584 30%→50%→70%→95%→100% sequentially at room temperature, and then dipped for
585 5 min three times with xylene. Finally, brains were mounted with DPX and allowed DPX

586 to dry for 2 days before imaging. Primary antibodies used were: chicken anti-GFP
587 (1:1000; Life Technologies #A10262), rabbit anti-GFP (1:1000; Life Technologies
588 #A11122), rabbit anti-RFP (1:1000; Life Technologies #R10367), rabbit anti-PTTH
589 antibody (1:1300), mouse anti-nc82 (1:40; DSHB), mouse anti-EcR-A (1:10;
590 AB_528214) and mouse anti-EcR-B1 (1:10; AB_2154902). Secondary antibodies used
591 were: Alexa Fluor goat anti-chicken 488 (1:500; Life Technologies #A11039), Alexa
592 Fluor goat anti-rabbit 488 (1:500; Life Technologies #A11034), Alexa Fluor goat anti-
593 rabbit 546 (1:500; Life Technologies #A11010), Alexa Fluor goat anti-mouse 647 (1:500;
594 Life Technologies #A21235), and Alexa Fluor goat anti-mouse 488 (1:500; Life
595 Technologies #A11029).
596
597 **Confocal microscopy and image analysis**
598
599 Confocal imaging was performed under an LSM 710 inverted confocal microscope
600 (ZEISS, Germany), with a Plan-Apochromat 20×/0.8 M27 objective or an EC Plan-
601 Neofluar 40x/1.30 oil DIC M27 objective, and later analyzed using Fiji software.
602
603 **Generation of anti-PTTH antibody**
604
605 The antisera used to recognize PTTH peptide were raised in New Zealand white rabbits
606 using the synthetic peptide N'- TSQSDHPYSWMNKDQPWQFKC -C'. The synthesis of
607 antigen peptide, the production and purification of antiserum were performed by Beijing
608 Genomics Institute (BGI).

609

610 **Generation of UAS-PTTH**

611

612 pJFRC28-5XUAS-IVS-GFP-p10 (#12073; Fungene Biotechnology, Shanghai, China)
613 was used for the generation of the pJFRC28-UAS-PTTH construct. The pJFRC28-
614 10XUAS-IVS-GFP-p10 plasmid was digested with NotI and XbaI to remove the GFP
615 coding sequence, and then the cDNA of PTTH was cloned into this plasmid by Gibson
616 Assembly. The Kozak sequence was added right upstream of the ATG. UAS-PTTH
617 constructs were injected and integrated into the attP2 site on the third chromosome
618 through phiC31 integrase mediated transgenesis. The construct was confirmed using
619 DNA sequencing through PCR. The primers used for cloning PTTH cDNA were as
620 follows:
621 UAS-PTTH-F
622 ATTCTTATCCTTTACTTCAGGCGGCCGCAAAATGGATATAAAAGTATGGCGACTCC
623 UAS-PTTH-R
624 GTTATTTTAAAAACGATTCATTCTAGATCACTTTGTGCAGAAGCAGCCG

625

626 **Genomic DNA extraction and RT-PCR**

627

628 Genomic DNA was extracted from 10 whole bodies of wandering flies using MightyPrep
629 reagent for DNA (Takara #9182). Whole body RNA was extracted from 10 whole bodies
630 of wandering flies using TRIzol (Ambion #15596018). cDNA was generated from total
631 RNA using the Prime Script reagent kit (Takara #RR047A). Candidates of *ΔPtth* were

632 characterized by the loss of DNA band in the deleted areas through PCR on the
633 genomic DNA and cDNA. Primer sequences used in Figure 1 are listed in **Table S1**.
634
635 **Measurements of pupariation timing and adult mass**
636
637 The flies were reared at 25°C and 60% humidity under a 12 hr light:12 hr dark cycle.
638 Two-hour time collections of embryos laid on standard food vials. Each vial contained
639 20-30 eggs. The range of time for pupariation were recorded for each vial. Sexed adults
640 of 24h-old were weighted in groups of ten flies using a NENVER-TP-214 microbalance
641 at the same time.
642
643 **Identification of sex in *Drosophila* larvae**
644
645 Third instar larvae can be sexed (True et al., 2014). Gonads are translucent and visible
646 in side view in the posterior third of the larva. The male gonads are about five times
647 bigger than the female gonads. The identified wandering female and male larvae were
648 reared in different vials for the subsequent experiments.
649
650 **Rescue by 20-hydroxyecdysone feeding**
651
652 Thirty freshly ecdysed *ΔPtth* L3 larvae, grown at 25°C and 60% humidity under a 12 hr
653 light:12 hr dark cycle, were washed with water and transferred to normal food for
654 additional aging. After 20 h, larvae were washed and transferred to a vial supplemented

655 with either 20-hydroxyecdysone (20E, Cayman #16145, dissolved in 95% ethanol, final
656 concentration 0.2 mg/ml) or 95% ethanol (same volume as 20E). The wild type larvae
657 were directly transferred to vials supplemented with 20E or 95% ethanol upon L3
658 ecdysis. Once seeded with L3 larvae, the vials were returned to 25°C and 60% humidity
659 under a 12 hr light:12 hr dark cycle.
660
661 **Quantification of fluorescence intensity**
662
663 The fluorescence intensity was quantified using Fiji software. The areas of interest
664 (ROI) were marked in the slices including the interested regions and quantified using
665 the "plot z-axis profile" function. The fluorescence intensity in each slice was summed
666 for statistics and plot. The parameters used for confocal imaging of each brain were the
667 same.
668
669 **Calcium imaging**
670
671 Flies aged 4-6 days were immobilized on ice for ~30 s. The brain was then dissected
672 out in extra-cellular solution (ECS) that contains (in millimoles): 108 NaCl, 5 KC1, 5
673 trehalose, 5 sucrose, 5 HEPES, 26 $NaHCO_3$, 1 NaH_2PO_4, 2 $CaCl_2$, and 1.5 $MgCl_2$ [pH
674 7.1 – 7.3 when bubbled with 95% (vol/vol) O_2/5% (vol/vol) CO_2, ~290 mOsm] and
675 mounted on a poly-D-lysine coated coverslip. The samples were continuously perfused
676 with ECS.
677

678 Calcium imaging was performed at 21°C on a customized two-photon microscope
679 equipped with a resonant scanner (Nikon), a piezo objective scanner (Nikon) and a 40x
680 water-immersion objective (Nikon). GCaMP6s was excited at 920 nm.
681
682 Analysis of calcium imaging data was done offline with NIS-Elements AR 5.30.01.
683 Briefly, the square region of interest (ROIs), 25 pixels on the pC1 neurons in the center
684 of lateral junction, was chosen for measurements. For each frame, the average
685 fluorescence intensity of pixels within ROIs was calculated blind to genotype. The
686 average fluorescence intensity of ROIs in each frame covering pC1 neurons were
687 summed for statistics and plot.
688
689 **RNA isolation and sequencing**
690
691 About 100 female fly brains were dissected from single individuals and the total RNA
692 was extracted using TRIzol (Ambion #15596018). Sequencing was performed on an
693 Illumina Novoseq6000 PE150 (Illumina, CA). Three biological replicates were performed
694 for each genetic type. The library preparation and sequencing were performed by
695 Novogene in China.
696
697 **RNA-seq analyses**
698
699 RNA-seq reads were mapped to the reference dmel-all-r6.42 (flaybase) using STAR
700 (v2.7.6a) (Dobin et al., 2013) with default parameters. Aligned reads were assigned to

701 dmel-all-r6.43.gtf gene annotation model, mapping reads were counted by
702 featureCounts from subread package with default parameters (Liao et al., 2013), and
703 then the transcript per millions (TPMs) was calculated. Differential expression was
704 analyzed with the DESeq2 package (Love et al., 2014) and visualized by volcano plots
705 using the maximum a posteriori estimated log-fold change using the $\log_2$(fold-change)
706 calculated from TPMs.
707
708 **qRT-PCR**
709
710 Whole brain RNA was extracted from about 100 fly brains using TRIzol (Ambion
711 #15596018). The cDNA was synthesized using Prime Script reagent kit (Takara
712 #RR047A). Quantitative PCR was performed on Thermo Piko Real 96 (Thermo) using
713 SYBR Green PCR Master Mix (Takara #RR820A). The mRNA expression level was
714 calculated by the $2^{-\Delta\Delta Ct}$ method and the results were plotted by using tubulin as the
715 reference gene. Primers are listed in **Table S1**. All reactions were performed in
716 triplicate. The average of four biological replicates ± SEM was plotted.
717
718 **Statistical analysis**
719
720 Statistical analyses were carried out using R software version 3.4.3 or Prism7
721 (GraphPad software). For the copulation rate, chi-square test is applied. The Mann-
722 Whitney U test was applied for analyzing the significance of two columns. Kruskal-

723 Wallis ANOVA test followed by post-hoc Mann-Whitney U test, was used to identify
724 significant differences between multiple groups.
725
726 **Data, Materials, and Software Availability**
727
728 All study data are included in the main text and supporting information, except for the
729 sequence data of RNAseq (**Supplementary File 3**) has been deposited in the Genome
730 Sequence Archive under the accession number CRA012130 in PRJCA018750. This
731 study does not involve new code. Fly stocks and reagents used in this study are
732 available from the corresponding author upon reasonable request.
733
734 **Acknowledgments**
735
736 We thank Yi Rao (Peking University), Yufeng Pan (Southeast University), Kaiyu Wang
737 (Lingang Laboratory), Yan Zhu (Chinese Academy of Sciences), Paul Garrity (Brandeis
738 University), Wei Zhang (Tsinghua University), Li Liu (Chinese Academy of Sciences)
739 and Xuan Guo (Jinzhou Medical University), the Bloomington Drosophila Stock Center
740 and Tsinghua Fly Center for sharing fly strains; Chenzhu Wang (Chinese Academy of
741 Sciences), Yufeng Pan (Southeast University) and Zhiqiang Yan (Shenzhen Bay
742 Laboratory) for their comments; Fengming Wu (Chinese Academy of Sciences), Tao
743 Wang (Chinese Academy of Sciences) and Jin Ge (Chinese Academy of Sciences) for
744 assistance with behavior assays; Yihui Chen for the maintenance of fly stocks; other
745 members of the Zhou laboratory for helpful discussions.

746 **References**

747 Avila F W, Sirot L K, LaFlamme B A, Rubinstein C D, & Wolfner M F. (2011). Insect seminal fluid
748 proteins: identification and function. *Annu Rev Entomol, 56*, 21-40.
749 doi:10.1146/annurev-ento-120709-144823
750 Billeter J C, Villella A, Allendorfer J B, Dornan A J, Richardson M, Gailey D A, & Goodwin S F.
751 (2006). Isoform-specific control of male neuronal differentiation and behavior in
752 Drosophila by the fruitless gene. *Curr Biol, 16*(11), 1063-1076.
753 doi:10.1016/j.cub.2006.04.039
754 Clowney E J, Iguchi S, Bussell J J, Scheer E, & Ruta V. (2015). Multimodal chemosensory circuits
755 controlling male courtship in Drosophila. *Neuron, 87*(5), 1036-1049.
756 doi:10.1016/j.neuron.2015.07.025
757 Connolly K, & Cook R. (1973). Rejection responses by female Drosophila-melanogaster - their
758 ontogeny, causality and effects upon behavior of courting male. *Behaviour, 44*(1-2), 142-
759 166. doi:10.1163/156853973x00364
760 Cubells J F, & Zabetian C P. (2004). Human genetics of plasma dopamine beta-hydroxylase
761 activity: applications to research in psychiatry and neurology. *Psychopharmacology*
762 *(Berl), 174*(4), 463-476. doi:10.1007/s00213-004-1840-8
763 Dai J D, & Gilbert L I. (1991). Metamorphosis of the corpus allatum and degeneration of the
764 prothoracic glands during the larval-pupal-adult transformation of Drosophila
765 melanogaster: a cytophysiological analysis of the ring gland. *Dev Biol, 144*(2), 309-326.
766 doi:10.1016/0012-1606(91)90424-2
767 Dalton J E, Lebo M S, Sanders L E, Sun F, & Arbeitman M N. (2009). Ecdysone receptor acts in
768 fruitless- expressing neurons to mediate drosophila courtship behaviors. *Curr Biol,*
769 *19*(17), 1447-1452. doi:10.1016/j.cub.2009.06.063
770 Demir E, & Dickson B J. (2005). fruitless splicing specifies male courtship behavior in Drosophila.
771 *Cell, 121*(5), 785-794. doi:10.1016/j.cell.2005.04.027
772 Deng B, Li Q, Liu X, Cao Y, Li B, Qian Y, Xu R, Mao R, Zhou E, Zhang W, Huang J, & Rao Y. (2019).
773 Chemoconnectomics: mapping chemical transmission in Drosophila. *Neuron, 101*(5),
774 876-893.e874. doi:10.1016/j.neuron.2019.01.045
775 Deutsch D, Pacheco D, Encarnacion-Rivera L, Pereira T, Fathy R, Clemens J, Girardin C, Calhoun
776 A, Ireland E, Burke A, Dorkenwald S, McKellar C, Macrina T, Lu R, Lee K, Kemnitz N, Ih D,
777 Castro M, Halageri A, Jordan C, Silversmith W, Wu J, Seung H S, & Murthy M. (2020). The
778 neural basis for a persistent internal state in Drosophila females. *Elife, 9*.
779 doi:10.7554/eLife.59502
780 Dickson B J. (2008). Wired for sex: the neurobiology of Drosophila mating decisions. *Science,*
781 *322*(5903), 904-909. doi:10.1126/science.1159276
782 Dobin A, Davis C A, Schlesinger F, Drenkow J, Zaleski C, Jha S, Batut P, Chaisson M, & Gingeras T
783 R. (2013). STAR: ultrafast universal RNA-seq aligner. *Bioinformatics, 29*(1), 15-21.
784 doi:10.1093/bioinformatics/bts635
785 Feng K, Palfreyman M T, Hasemeyer M, Talsma A, & Dickson B J. (2014). Ascending SAG neurons
786 control sexual receptivity of Drosophila females. *Neuron, 83*(1), 135-148.
787 doi:10.1016/j.neuron.2014.05.017

Ferveur J F. (2010). Drosophila female courtship and mating behaviors: sensory signals, genes, neural structures and evolution. *Curr Opin Neurobiol, 20*(6), 764-769. doi:10.1016/j.conb.2010.09.007

Fuyama Y, & Ueyama M. (1997). Ovulation and the suppression of mating in Drosophila melanogaster females: behavioral basis. *Behav Genet, 27*(5), 483-488. doi:10.1023/a:1025630602057

Ganter G K, Walton K L, Merriman J O, Salmon M V, Brooks K M, Maddula S, & Kravitz E A. (2007). Increased male-male courtship in ecdysone receptor deficient adult flies. *Behav Genet, 37*(3), 507-512. doi:10.1007/s10519-006-9140-1

Greenspan R J, & Ferveur J F. (2000). Courtship in Drosophila. *Annu Rev Genet, 34*, 205-232. doi:10.1146/annurev.genet.34.1.205

Hall J. (1978). Courtship among males due to a male-sterile mutation in Drosophila melanogaster. *Behavior Genetics,* 8(2), 125-41. doi:10.1007/BF01066870

Hall J C. (1994). The mating of a fly. *Science, 264*(5166), 1702-1714. doi:10.1126/science.8209251

Hamada F N, Rosenzweig M, Kang K, Pulver S R, Ghezzi A, Jegla T J, & Garrity P A. (2008). An internal thermal sensor controlling temperature preference in Drosophila. *Nature, 454*(7201), 217-220. doi:10.1038/nature07001

Häsemeyer M, Yapici N, Heberlein U, & Dickson B J. (2009). Sensory neurons in the Drosophila genital tract regulate female reproductive behavior. *Neuron, 61*(4), 511-518. doi:10.1016/j.neuron.2009.01.009

Herbison A E. (2016). Control of puberty onset and fertility by gonadotropin-releasing hormone neurons. *Nat Rev Endocrinol, 12*(8), 452-466. doi:10.1038/nrendo.2016.70

Hoopfer E D, Jung Y, Inagaki H K, Rubin G M, & Anderson D J. (2015). P1 interneurons promote a persistent internal state that enhances inter-male aggression in Drosophila. *Elife, 4*. doi:10.7554/eLife.11346

Imura E, Shimada-Niwa Y, Nishimura T, Huckesfeld S, Schlegel P, Ohhara Y, Kondo S, Tanimoto H, Cardona A, Pankratz M J, & Niwa R. (2020). The Corazonin-PTTH neuronal axis controls systemic body growth by regulating basal ecdysteroid biosynthesis in Drosophila melanogaster. *Curr Biol, 30*(11), 2156-2165 e2155. doi:10.1016/j.cub.2020.03.050

Ishimoto H, & Kamikouchi A. (2020). A feedforward circuit regulates action selection of pre-mating courtship behavior in female Drosophila. *Curr Biol, 30*(3), 396-407.e394. doi:10.1016/j.cub.2019.11.065

Ito H, Sato K, Koganezawa M, Ote M, Matsumoto K, Hama C, & Yamamoto D. (2012). Fruitless recruits two antagonistic chromatin factors to establish single-neuron sexual dimorphism. *Cell, 149*(6), 1327-1338. doi:10.1016/j.cell.2012.04.025

Jang Y H, Chae H S, & Kim Y J. (2017). Female-specific myoinhibitory peptide neurons regulate mating receptivity in Drosophila melanogaster. *Nat Commun, 8*(1), 1630. doi:10.1038/s41467-017-01794-9

Kim C H, Zabetian C P, Cubells J F, Cho S, Biaggioni I, Cohen B M, Robertson D, & Kim K S. (2002). Mutations in the dopamine beta-hydroxylase gene are associated with human norepinephrine deficiency. *Am J Med Genet, 108*(2), 140-147.

831 Kimura K, Hachiya T, Koganezawa M, Tazawa T, & Yamamoto D. (2008). Fruitless and doublesex
832 coordinate to generate male-specific neurons that can initiate courtship. *Neuron, 59*(5),
833 759-769. doi:10.1016/j.neuron.2008.06.007
834 Kimura K, Sato C, Koganezawa M, & Yamamoto D. (2015). Drosophila ovipositor extension in
835 mating behavior and egg deposition involves distinct sets of brain interneurons. *PLoS*
836 *One, 10*(5), e0126445. doi:10.1371/journal.pone.0126445
837 Kohatsu S, Koganezawa M, & Yamamoto D. (2011). Female contact activates male-specific
838 interneurons that trigger stereotypic courtship behavior in Drosophila. *Neuron, 69*(3),
839 498-508. doi:10.1016/j.neuron.2010.12.017
840 Kubli E. (2003). Sex-peptides: seminal peptides of the Drosophila male. *Cell Mol Life Sci, 60*(8),
841 1689-1704. doi:10.1007/s00018-003-3052
842 Kurtovic A, Widmer A, & Dickson B J. (2007). A single class of olfactory neurons mediates
843 behavioural responses to a Drosophila sex pheromone. *Nature, 446*(7135), 542-546.
844 doi:10.1038/nature05672
845 Kvitsiani D, & Dickson B J. (2006). Shared neural circuitry for female and male sexual behaviours
846 in Drosophila. *Curr Biol, 16*(10), R355-356. doi:10.1016/j.cub.2006.04.025
847 Lavrynenko O, Rodenfels J, Carvalho M, Dye N A, Lafont R, Eaton S, & Shevchenko A. (2015).
848 The ecdysteroidome of Drosophila: influence of diet and development. *Development,*
849 *142*(21), 3758-3768. doi:10.1242/dev.124982
850 Liao Y, Smyth G K, & Shi W. (2013). The Subread aligner: fast, accurate and scalable read
851 mapping by seed-and-vote. *Nucleic Acids Res, 41*(10), e108. doi:10.1093/nar/gkt214
852 Love M I, Huber W, & Anders S. (2014). Moderated estimation of fold change and dispersion for
853 RNA-seq data with DESeq2. *Genome Biol, 15*(12), 550. doi:10.1186/s13059-014-0550-8
854 Ma B, Wang R, Liu Y, Deng B, Wang T, Wu F, & Zhou C. (2022). Serotonin signaling modulates
855 sexual receptivity of virgin female Drosophila. *Neurosci Bull, 38*(11), 1277-1291.
856 doi:10.1007/s12264-022-00908-8
857 Manoli D S, Fan P, Fraser E J, & Shah N M. (2013). Neural control of sexually dimorphic
858 behaviors. *Curr Opin Neurobiol, 23*(3), 330-338. doi:10.1016/j.conb.2013.04.005
859 Manoli D S, Foss M, Villella A, Taylor B J, Hall J C, & Baker B S. (2005). Male-specific fruitless
860 specifies the neural substrates of Drosophila courtship behaviour. *Nature, 436*(7049),
861 395-400. doi:10.1038/nature03859
862 Manoli D S, Meissner G W, & Baker B S. (2006). Blueprints for behavior: genetic specification of
863 neural circuitry for innate behaviors. *Trends Neurosci, 29*(8), 444-451.
864 doi:10.1016/j.tins.2006.06.006
865 McBrayer Z, Ono H, Shimell M, Parvy J P, Beckstead R B, Warren J T, Thummel C S, Dauphin-
866 Villemant C, Gilbert L I, & O'Connor M B. (2007a). Prothoracicotropic hormone regulates
867 developmental timing and body size in Drosophila. *Dev Cell, 13*(6), 857-871.
868 doi:10.1016/j.devcel.2007.11.003
869 Mcbrayer Z, Ono H, Shimell M J, Parvy J P, Beckstead R B, Warren J T, Thummel C S, Dauphin-
870 Villemant C, Gilbert L I, & O'Connor M B. (2007b). Prothoracicotropic hormone regulates
871 developmental timing and body size in Drosophila. *Developmental Cell, 13*(6), 857-871.
872 doi:10.1016/j.devcel.2007.11.003

McGuire S E, Mao Z, & Davis R L. (2004). Spatiotemporal gene expression targeting with the TARGET and gene-switch systems in Drosophila. *Sci STKE, 2004*(220), pl6. doi:10.1126/stke.2202004pl6

Mellert D J, Knapp J M, Manoli D S, Meissner G W, & Baker B S. (2010). Midline crossing by gustatory receptor neuron axons is regulated by fruitless, doublesex and the Roundabout receptors. *Development, 137*(2), 323-332. doi:10.1242/dev.045047

Mellert D J, Robinett C C, & Baker B S. (2012). doublesex functions early and late in gustatory sense organ development. *PLoS One, 7*(12), e51489. doi:10.1371/journal.pone.0051489

Mezzera C, Brotas M, Gaspar M, Pavlou H J, Goodwin S F, & Vasconcelos M L. (2020). Ovipositor extrusion promotes the transition from courtship to copulation and signals female acceptance in Drosophila melanogaster. *Curr Biol, 30*(19), 3736-3748.e3735. doi:10.1016/j.cub.2020.06.071

Neckameyer W S. (1998). Dopamine modulates female sexual receptivity in Drosophila melanogaster. *J Neurogenet, 12*(2), 101-114. doi:10.3109/01677069809167259

Yamanaka, N, Romero, N M, Martin, F A, Rewitz, K F, Sun, M, O'Connor, & M B, Léopold, P. (2013). Neuroendocrine control of Drosophila larval light preference. *Science,* 341(6150), 1113-1116. doi: 10.1126/science.1241210

Pan X, & O'Connor M B. (2019). Developmental maturation: Drosophila asta signaling provides a kiss to grow up. *Curr Biol, 29*(5), R161-R164. doi:10.1016/j.cub.2019.01.040

Pan Y, & Baker B S. (2014). Genetic identification and separation of innate and experience-dependent courtship behaviors in Drosophila. *Cell, 156*(1-2), 236-248. doi:10.1016/j.cell.2013.11.041

Pan Y, Meissner G W, & Baker B S. (2012). Joint control of Drosophila male courtship behavior by motion cues and activation of male-specific P1 neurons. *PNAS, 109*(25), 10065-10070. doi:10.1073/pnas.1207107109

Pan Y, Robinett C C, & Baker B S. (2011). Turning males on: activation of male courtship behavior in Drosophila melanogaster. *PLoS One, 6*(6), e21144. doi:10.1371/journal.pone.0021144

Park D H, Kashimoto T, Ebstein R P, & Goldstein M. (1976). Purification and immunochemical characterization of dopamine beta-hydroxylase from human pheochromocytoma. *Mol Pharmacol, 12*(1), 73-81.

Pavlou H J, & Goodwin S F. (2013). Courtship behavior in Drosophila melanogaster: towards a 'courtship connectome'. *Curr Opin Neurobiol, 23*(1), 76-83. doi:10.1016/j.conb.2012.09.002

Pfeiffer B D, Jenett A, Hammonds A S, Ngo T T, Misra S, Murphy C, Scully A, Carlson J W, Wan K H, Laverty T R, Mungall C, Svirskas R, Kadonaga J T, Doe C Q, Eisen M B, Celniker S E, & Rubin G M. (2008). Tools for neuroanatomy and neurogenetics in Drosophila. *PNAS, 105*(28), 9715-9720. doi:10.1073/pnas.0803697105

Pfeiffer B D, Ngo T T, Hibbard K L, Murphy C, Jenett A, Truman J W, & Rubin G M. (2010). Refinement of tools for targeted gene expression in Drosophila. *Genetics, 186*(2), 735-755. doi:10.1534/genetics.110.119917

Prigge S T, Mains R E, Eipper B A, & Amzel L M. (2000). New insights into copper monooxygenases and peptide amidation: structure, mechanism and function. *Cell Mol Life Sci, 57*(8-9), 1236-1259. doi:10.1007/pl00000763

Rewitz K F, Yamanaka N, Gilbert L I, & O'Connor M B. (2009). The insect neuropeptide PTTH activates receptor tyrosine kinase torso to initiate metamorphosis. *Science, 326*(5958), 1403-1405. doi:10.1126/science.1176450

Rezával C, Nojima T, Neville M C, Lin A C, & Goodwin S F. (2014). Sexually dimorphic octopaminergic neurons modulate female postmating behaviors in Drosophila. *Curr Biol, 24*(7), 725-730. doi:10.1016/j.cub.2013.12.051

Rezával C, Pattnaik S, Pavlou H J, Nojima T, Brüggemeier B, D'Souza L A D, Dweck H K M, & Goodwin S F. (2016). Activation of latent courtship circuitry in the brain of Drosophila females induces male-like behaviors. *Curr Biol, 26*(18), 2508-2515. doi:10.1016/j.cub.2016.07.021

Riddiford L M, Cherbas P, & Truman J W. (2000). Ecdysone receptors and their biological actions. *Vitam Horm, 60*, 1-73. doi:10.1016/s0083-6729(00)60016-x

Rideout E J, Dornan A J, Neville M C, Eadie S, & Goodwin S F. (2010). Control of sexual differentiation and behavior by the doublesex gene in Drosophila melanogaster. *Nat Neurosci, 13*(4), 458-466. doi:10.1038/nn.2515

Roy S, Saha T T, Zou Z, & Raikhel A S. (2018). Regulatory pathways controlling female insect reproduction. *Annu Rev Entomol, 63*, 489-511. doi:10.1146/annurev-ento-020117-043258

Ruta V, Datta S R, Vasconcelos M L, Freeland J, Looger L L, & Axel R. (2010). A dimorphic pheromone circuit in Drosophila from sensory input to descending output. *Nature, 468*(7324), 686-690. doi:10.1038/nature09554

Scheffer L K, Xu C S, Januszewski M, Lu Z, Takemura S Y, Hayworth K J, Huang G B, Shinomiya K et al. & Plaza S M. (2020). A connectome and analysis of the adult Drosophila central brain. *Elife, 9*. doi:10.7554/eLife.57443

Schretter C E, Aso Y, Robie A A, Dreher M, Dolan M J, Chen N, Ito M, Yang T, Parekh R, Branson K M, & Rubin G M. (2020). Cell types and neuronal circuitry underlying female aggression in Drosophila. *Elife, 9*. doi:10.7554/eLife.58942

Sengupta S, Chan Y B, Palavicino-Maggio C B, & Kravitz E A. (2022). GABA transmission from mAL interneurons regulates aggression in Drosophila males. *PNAS, 119*(5). doi:10.1073/pnas.2117101119

Shimell M, Pan X, Martin F A, Ghosh A C, Leopold P, O'Connor M B, & Romero N M. (2018). Prothoracicotropic hormone modulates environmental adaptive plasticity through the control of developmental timing. *Development, 145*(6). doi:10.1242/dev.159699

Siwicki K K, & Kravitz E A. (2009). Fruitless, doublesex and the genetics of social behavior in Drosophila melanogaster. *Curr Opin Neurobiol, 19*(2), 200-206. doi:10.1016/j.conb.2009.04.001

Stockinger P, Kvitsiani D, Rotkopf S, Tirián L, & Dickson B J. (2005). Neural circuitry that governs Drosophila male courtship behavior. *Cell, 121*(5), 795-807. doi:10.1016/j.cell.2005.04.026

Taisz I, Donà E, Münch D, Bailey S N, Morris B J, Meechan K I, Stevens K M, Varela-Martínez I, Gkantia M, Schlegel P, Ribeiro C, Jefferis G, & Galili D S. (2023). Generating parallel representations of position and identity in the olfactory system. *Cell, 186*(12), 2556-2573.e2522. doi:10.1016/j.cell.2023.04.038

Terhzaz S, Rosay P, Goodwin S F, & Veenstra J A. (2007). The neuropeptide SIFamide modulates sexual behavior in Drosophila. *Biochem Biophys Res Commun, 352*(2), 305-310. doi:10.1016/j.bbrc.2006.11.030

Timmers H J, Deinum J, Wevers R A, & Lenders J W. (2004). Congenital dopamine-beta-hydroxylase deficiency in humans. *Ann N Y Acad Sci, 1018*, 520-523. doi:10.1196/annals.1296.064

Sylwester Chyb and Nicolas Gompel. (2014). Atlas of Drosophila morphology: wild-type and classical mutants. "Life stages: third instar larva and pupa". Elsevier, pp. 18-19.

Truman J W, & Riddiford L M. (2023). Drosophila postembryonic nervous system development: a model for the endocrine control of development. *Genetics, 223*(3). doi:10.1093/genetics/iyac184

Truman J W, Talbot W S, Fahrbach S E, & Hogness D S. (1994). Ecdysone receptor expression in the CNS correlates with stage-specific responses to ecdysteroids during Drosophila and Manduca development. *Development, 120*(1), 219-234. doi:10.1242/dev.120.1.219

Tsuneoka Y, Tsukahara S, Yoshida S, Takase K, Oda S, Kuroda M, & Funato H. (2017). Moxd1 is a marker for sexual dimorphism in the medial preoptic area, Bed Nucleus of the Stria Terminalis and Medial Amygdala. *Front Neuroanat, 11*, 26. doi:10.3389/fnana.2017.00026

Vendelboe T V, Harris P, Zhao Y, Walter T S, Harlos K, El Omari K, & Christensen H E. (2016). The crystal structure of human dopamine β-hydroxylase at 2.9 Å resolution. *Sci Adv, 2*(4), e1500980. doi:10.1126/sciadv.1500980

von Philipsborn A C, Liu T, Yu J Y, Masser C, Bidaye S S, & Dickson B J. (2011). Neuronal control of Drosophila courtship song. *Neuron, 69*(3), 509-522. doi:10.1016/j.neuron.2011.01.011

Wang F, Wang K, Forknall N, Parekh R, & Dickson B J. (2020a). Circuit and behavioral mechanisms of sexual rejection by Drosophila females. *Curr Biol, 30*(19), 3749-3760 e3743. doi:10.1016/j.cub.2020.07.083

Wang F, Wang K, Forknall N, Patrick C, Yang T, Parekh R, Bock D, & Dickson B J. (2020b). Neural circuitry linking mating and egg laying in Drosophila females. *Nature, 579*(7797), 101-105. doi:10.1038/s41586-020-2055-9

Wang K, Wang F, Forknall N, Yang T, Patrick C, Parekh R, & Dickson B J. (2021). Neural circuit mechanisms of sexual receptivity in Drosophila females. *Nature, 589*(7843), 577-581. doi:10.1038/s41586-020-2972-7

Wang L, & Anderson D J. (2010). Identification of an aggression-promoting pheromone and its receptor neurons in Drosophila. *Nature, 463*(7278), 227-231. doi:10.1038/nature08678

Wang T, Jing B, Deng B, Shi K, Li J, Ma B, Wu F, & Zhou C. (2022). Drosulfakinin signaling modulates female sexual receptivity in Drosophila. *Elife, 11*. doi:10.7554/eLife.76025

Wu Y, Bidaye S, & Mahringer D. (2019). Drosophila female-specific brain neuron elicits persistent position- and direction-selective male-like social behaviors. doi:10.1101/594960

Xin X, Mains R E, & Eipper B A. (2004). Monooxygenase X, a member of the copper-dependent monooxygenase family localized to the endoplasmic reticulum. *J Biol Chem, 279*(46), 48159-48167. doi:10.1074/jbc.M407486200

1003 Yamamoto D. (2007). The neural and genetic substrates of sexual behavior in Drosophila. *Adv*
1004 *Genet, 59*, 39-66. doi:10.1016/S0065-2660(07)59002-4
1005 Yamamoto D, & Koganezawa M. (2013). Genes and circuits of courtship behaviour in Drosophila
1006 males. *Nat Rev Neurosci, 14*(10), 681-692. doi:10.1038/nrn3567
1007 Yamanaka N, Romero N M, Martin F A, Rewitz K F, Sun M, O'Connor M B, & Léopold P. (2013).
1008 Neuroendocrine control of Drosophila larval light preference. *Science, 341*(6150), 1113-
1009 1116. doi:10.1126/science.1241210
1010 Yang C H, Rumpf S, Xiang Y, Gordon M D, Song W, Jan L Y, & Jan Y N. (2009). Control of the
1011 postmating behavioral switch in Drosophila females by internal sensory neurons.
1012 *Neuron, 61*(4), 519-526. doi:10.1016/j.neuron.2008.12.021
1013 Zhou C, Pan Y, Robinett C C, Meissner G W, & Baker B S. (2014). Central brain neurons
1014 expressing doublesex regulate female receptivity in Drosophila. *Neuron, 83*(1), 149-163.
1015 doi:10.1016/j.neuron.2014.05.038
1016
1017
1018
1019
1020
1021
1022
1023
1024
1025
1026
1027
1028
1029
1030
1031
1032

1033 **Figure Legends**

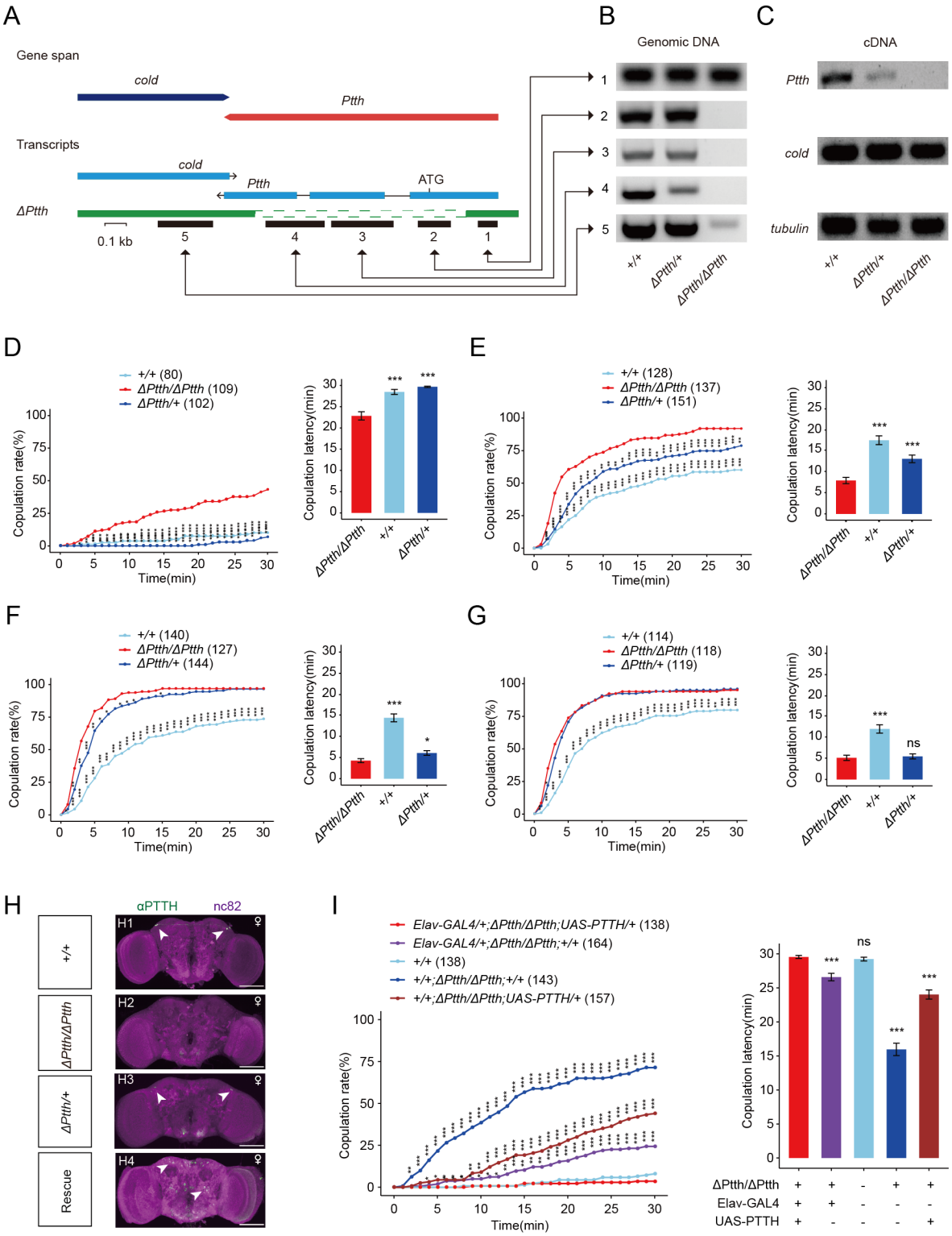

1034

1035 **Figure 1 *Ptth* null mutants have increased virgin female receptivity.**

1036 (A-C) Generation and validation of a 974 bp deletion mutant of the *Ptth* gene. (D-G)
1037 Virgin female receptivity of *Ptth* null mutants on the 1st (D), 2nd (E), 3rd (F) and 6th day
1038 (G) respectively. (H) Brain of indicated genotype, immunostained with anti-PTTH
1039 antibody (green) and counterstained with nc82 (magenta). Arrows show signals (green)
1040 stained with anti-PTTH antibody. Scale bars, 50 μm. (I) Enhanced virgin female
1041 receptivity of *ΔPtth* null mutants was rescued by elavGAL4 driving UAS-PTTH. The
1042 increased copulation rate and decreased latency to copulation on the 1st day after
1043 eclosion were rescued to the comparable level of control. The number of female flies
1044 paired with wild type males is displayed in parentheses. For the copulation rate, chi-
1045 square test is applied. For the latency to copulation, Kruskal-Wallis ANOVA and post
1046 hoc Mann-Whitney U tests are applied. Error bars indicate SEM. *$p < 0.05$, **$p < 0.01$,
1047 ***$p < 0.001$, ****$p < 0.0001$, ns indicates no significant difference.
1048
1049
1050
1051
1052
1053
1054
1055
1056
1057
1058
1059

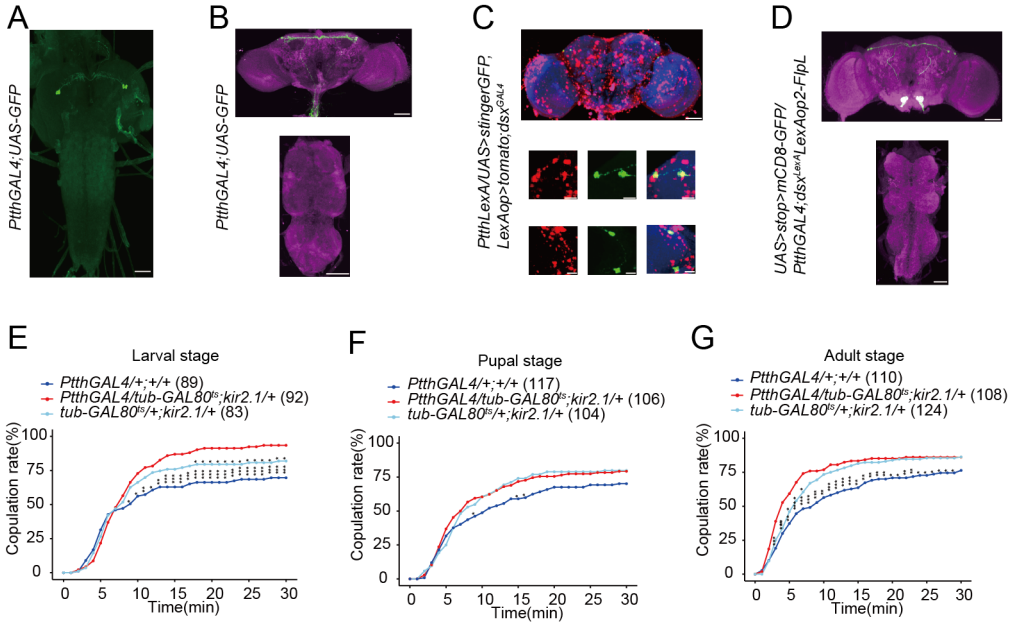

Figure 2 Inactivation of doublesex-positive PG neurons expressing PTTH enhances virgin female receptivity during the larval stage.

(A-B) Expression pattern of PtthGAL4 revealed by anti-GFP in larvae central nervous system (CNS) (A) and adult CNS (B). Representative of five female flies. Scale bars, 50 μm. (C) All PG neurons were colabeled by dsxGAL4 driving UAS-GFPStinger (red) and PtthLexA driving LexAop-tomato (green). Representative of five female brains. Scale bars, 50 μm and 5 μm (zoom-in). (D) All PG neurons were *Ptth* and *Dsx* co-expressing, labeled by intersectional strategy. Representative of 5 female brains. Scale bars, 50 μm. (E-G) PG neurons were inactivated during larval (E), pupal (F) and adult (G) stages respectively by kir2.1, restricted by shifts from 18°C to 30°C. The inactivation during the larval stage significantly increased the copulation rate (E). The number of female flies paired with wild-type males is displayed in parentheses. For the copulation rate, chi-square test is applied. Error bars indicate SEM. *$p < 0.05$, **$p < 0.01$, ***$p < 0.001$, ****$p < 0.0001$, ns indicates no significant difference.

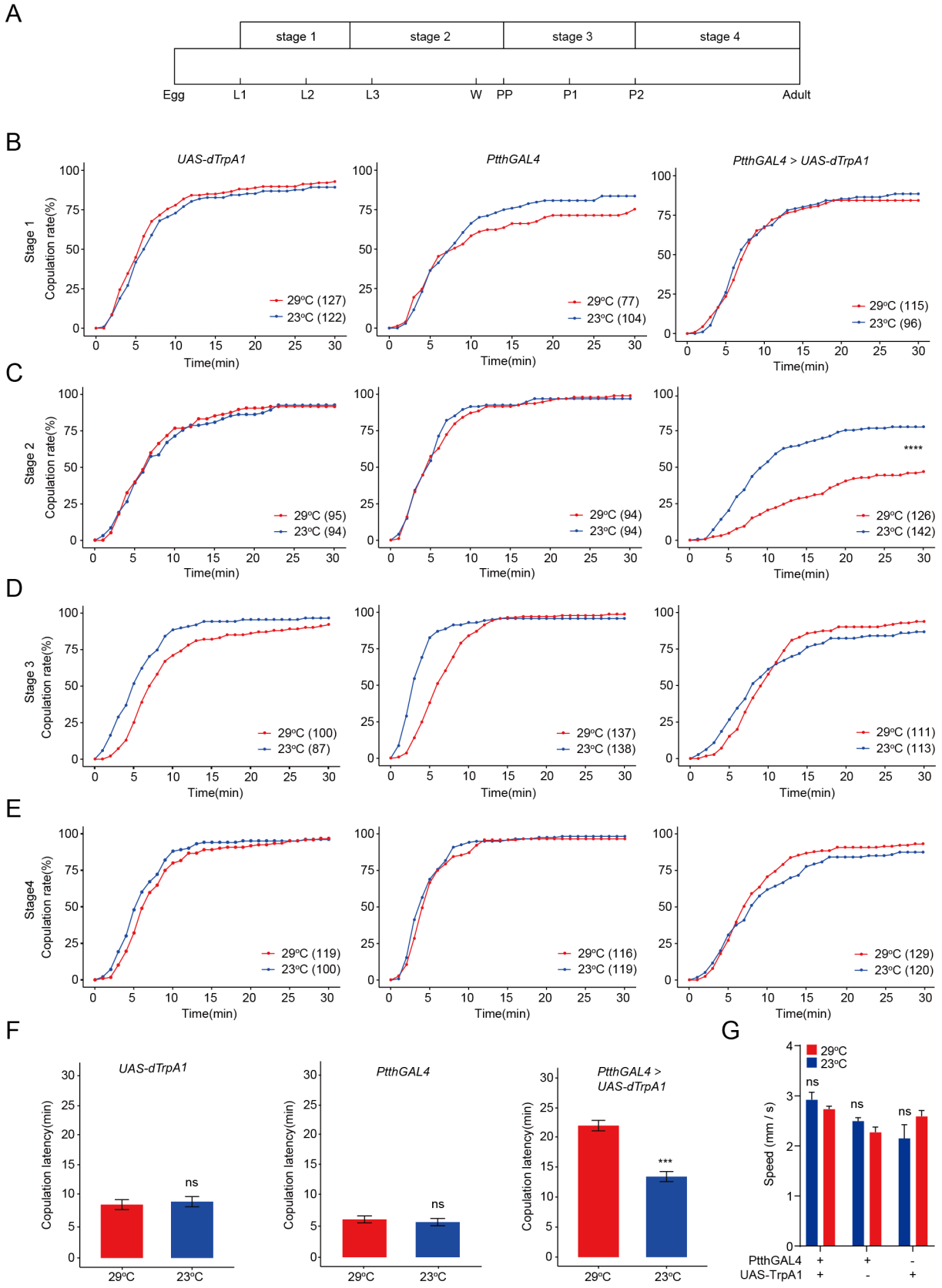
A
stage 1
stage 2
stage 3
stage 4
Egg
L1
L2
L3
W
PP
P1
P2
Adult
B
UAS-dTrpA1
PtthGAL4
PtthGAL4 > UAS-dTrpA1
Stage 1
Copulation rate(%)
Time(min)
29ºC (127)
23ºC (122)
29ºC (77)
23ºC (104)
29ºC (115)
23ºC (96)
C
Stage 2
29ºC (95)
23ºC (94)
29ºC (94)
23ºC (94)
****
29ºC (126)
23ºC (142)
D
Stage 3
29ºC (100)
23ºC (87)
29ºC (137)
23ºC (138)
29ºC (111)
23ºC (113)
E
Stage4
29ºC (119)
23ºC (100)
29ºC (116)
23ºC (119)
29ºC (129)
23ºC (120)
F
Copulation latency(min)
ns
***
29ºC
23ºC
G
Speed (mm / s)
PtthGAL4
UAS-TrpA1

1078 **Figure 3 Activation of PG neurons expressing PTTH during the 3rd-instar larvae**
1079 **inhibits virgin female receptivity.**
1080 (A) Four developmental stages of *Drosophila* before eclosion when PG neurons were
1081 thermogenetic activated by dTrpA1. L1, L2, and L3: start of three larval stages, W: start
1082 of wandering stage, Pp: puparium formation, P1 and P2: start of the 1st and 2nd day of
1083 pupal stage. (B-E) PtthGAL4 driving UAS-dTrpA1 activated PG neurons at 29°C.
1084 Activation of PG neurons at the stage 2 significantly decreased copulation rate (C), but
1085 not at the stage 1 (B), stage 3 (D) and stage 4 (E). (F) Activation of PG neurons at the
1086 stage 2 significantly increased the latency to copulation. (G) Mean velocity had no
1087 significant change when PG neurons were activated during the stage 2 compared with
1088 control females (ns = not significant, Kruskal-Wallis ANOVA and post hoc Mann-
1089 Whitney U tests, mean ± SEM, n = 8-12). The number of female flies paired with wild-
1090 type males is displayed in parentheses. For the copulation rate, chi-square test is
1091 applied. For the latency to copulation, Mann-Whitney U test is applied. Error bars
1092 indicate SEM. *$p < 0.05$, **$p < 0.01$, ***$p < 0.001$, ****$p < 0.0001$, ns indicates no
1093 significant difference.
1094
1095
1096
1097
1098
1099
1100
1101
1102
1103
1104
1105
1106
1107

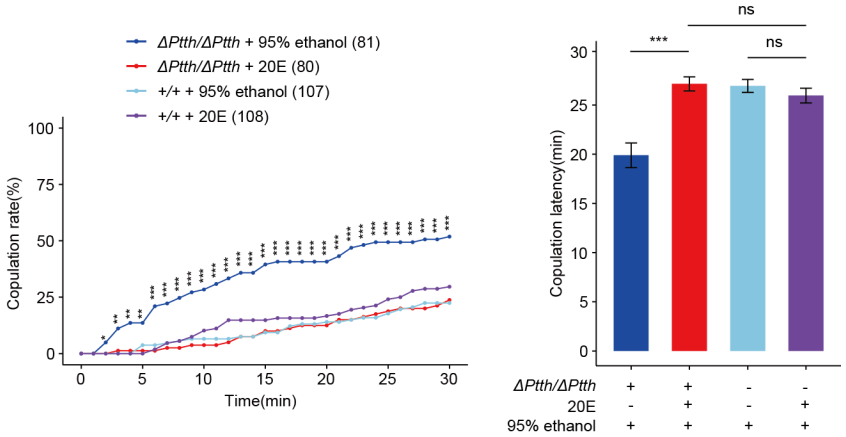

Figure 4 Feeding 20E restores virgin female receptivity of *Ptth* null mutant flies. (A-B) The increased copulation rate and decreased latency to copulation of the 24h-old *ΔPtth* flies were rescued to the comparable level of wild type females by feeding 20E to the 3rd-instar larval *ΔPtth* flies. The wild type larval females fed by 20E had no significantly different copulation rate and latency to copulation compared with the wild type females fed by the same volume of 95% ethanol which is the solvent of 20E. The number of female flies paired with wild-type males is displayed in parentheses. For the copulation rate, chi-square test is applied. For the latency to copulation, Kruskal-Wallis ANOVA and post hoc Mann-Whitney U tests are applied. Error bars indicate SEM. *p < 0.05, **p < 0.01, ***p < 0.001, ****p < 0.0001, ns indicates no significant difference.

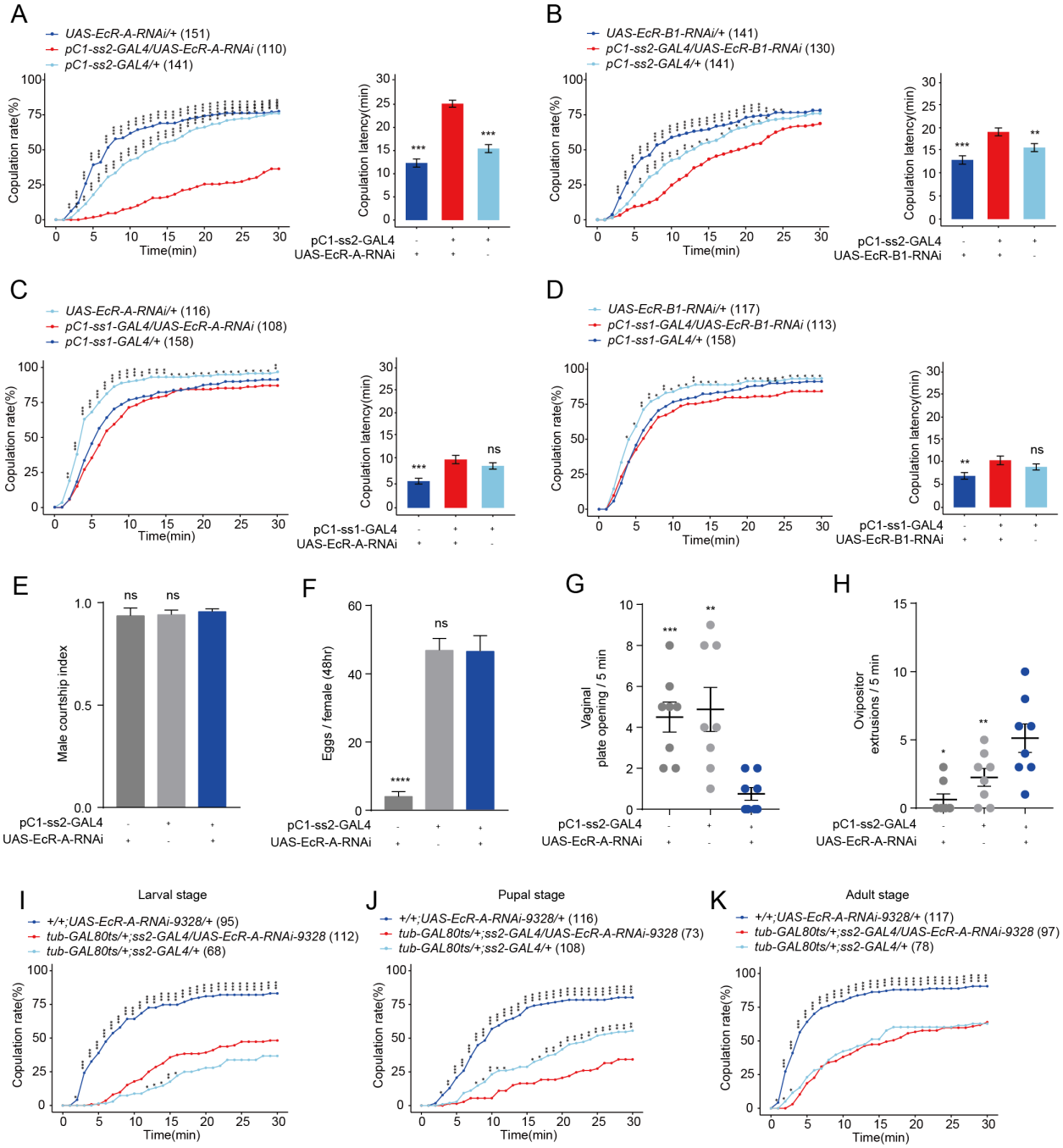

Figure 5 Virgin females with reduced EcR-A in pC1 neurons have reduced sexual receptivity.

(A) Knock-down of EcR-A in pC1 neurons driven by pC1-ss2-GAL4 significantly decreased the copulation rate and increased the latency to copulation. (B) Knock-down of EcR-B1 in pC1 neurons driven by pC1-ss2-GAL4 significantly prolonged the latency to copulation. (C-D) Knock-down of EcR-A (C) or EcR-B1 (D) in pC1 neurons driven by

1139 pC1-ss1-GAL4 did not affect the copulation rate or the latency to copulation. (E)
1140 Courtship index of wild-type males towards a female with the indicated genotype (n =
1141 8). (F) The number of eggs laid by virgin females during the 3rd - 4th day after eclosion
1142 when EcR-A was knocked down in pC1 neurons (n = 17-36). (G) Knock-down of EcR-A
1143 in pC1 neurons decreased the opening of vaginal plate of virgin females compared with
1144 controls (n = 8). (H) Knock-down of EcR-A in pC1 neurons increased the ovipositor
1145 extrusion of virgin females compared with controls (n = 8). (I-K) Virgin female copulation
1146 rate when EcR-A was knocked down in pC1 neurons temporally restricted by shifts from
1147 18°C to 30°C. EcR-A was knocked down during larval (I), pupal (J) and adult (K) stages
1148 respectively. Knock-down of EcR-A during pupal stage significantly decreased the
1149 copulation rate (J). The number of female flies paired with wild-type males is displayed
1150 in parentheses. For the copulation rate, chi-square test is applied. For other
1151 comparisons, Kruskal-Wallis ANOVA and post hoc Mann-Whitney U tests are applied.
1152 Error bars indicate SEM. *$p < 0.05$, **$p < 0.01$, ***$p < 0.001$, ****$p < 0.0001$, ns indicates
1153 no significant difference.
1154
1155
1156
1157
1158
1159
1160
1161
1162
1163
1164
1165
1166
1167
1168
1169

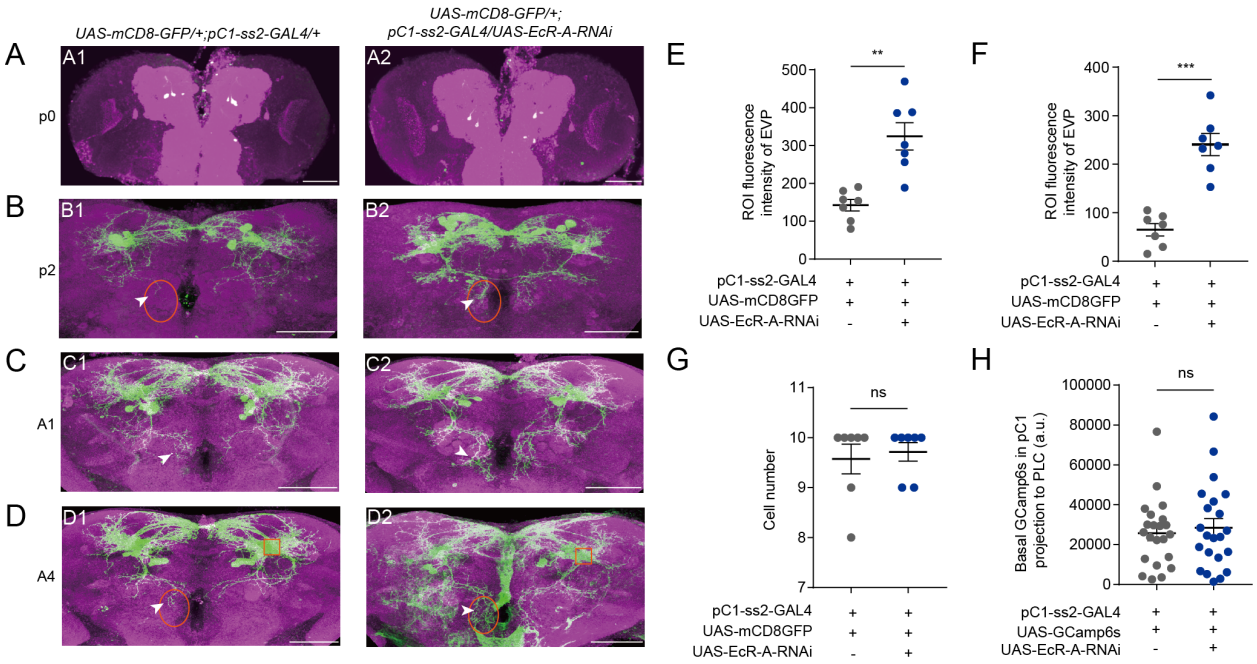

Figure 6 Reduced EcR-A in pC1 neurons induces the morphological changes. (A1-A2) pC1 neurons appeared at the start of the pupal stage. (B-D) Reduced EcR-A in pC1 neurons induced more elaborated morphologies of pC1d axons, especially the extra vertical projection (EVP). The EVP regions of pC1d neurons was indicated by arrows. The morphological changes appeared on the 2nd day of the pupal stage (B1-B2) and retained to the adult stage including the 1st day (C1-C2) and the 4th day (D1-D2) of the adult stage. p0, the 1st day of the pupal stage; p2, the 2nd day of the pupal stage; A1, the 1st day of the adult stage; A4, the 4th day of the adult stage. (E-F) Fluorescence intensity of EVP in pC1d neurons on the 2nd day of the pupal stage (E) and the 4th day of the adult stage (F) was quantified when EcR-A was reduced in pC1 neurons (n=7). The quantified EVP regions were marked in (B) and (D) with orange ellipses. (G) pC1 neurons of the 4th day adults had comparable cell body number when EcR-A was reduced in pC1 neurons or not (n = 7). (H) Basal GCaMP6s signals in the LPC region of pC1 neurons when EcR-A was reduced in pC1 neurons (n = 22). LPC regions, the neurites extending from pC1 cell bodies, were marked with orange square in (D1) and (D2). Scale bars are 50 μm. For all comparisons, Mann-Whitney U test is applied. Error bars indicate SEM. *$p < 0.05$, **$p < 0.01$, ***$p < 0.001$, ****$p < 0.0001$, ns indicates no significant difference.

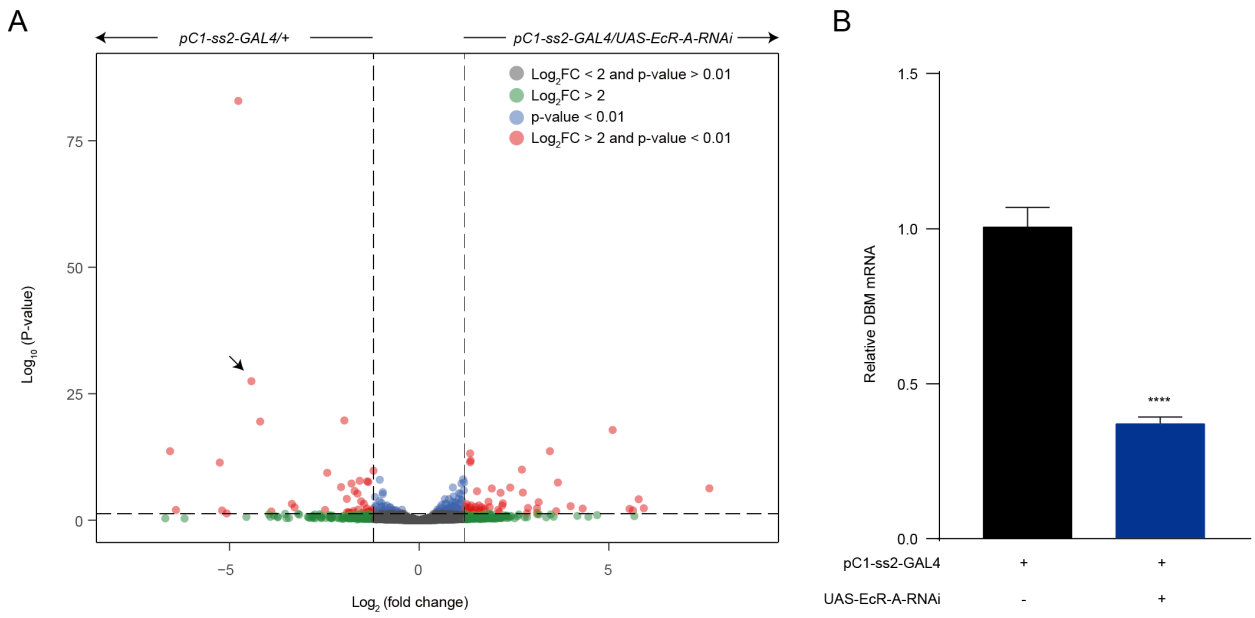

Figure 7 Reduced EcR-A in pC1 neurons induces the down-regulated dopamine beta-monooxygenase (DBM) level.

(A) Volcano plot of RNA-seq from virgin female brains in which EcR-A was knocked down in pC1 neurons or not. Each circle represents a protein-coding gene. Differential genes with a p-value < 0.01 are highlighted in blue. Differential genes with a fold change > 4 are highlighted in green. Differential genes with a p-value < 0.01 and fold change > 4 are highlighted in red. DBM, the most down-regulated genes with annotation, are indicated by black arrow. Data are from three replicates, each contains about 100 brains. (B) qRT-PCR for DBM when EcR-A was knocked down in pC1 neurons. Bars represent mean ± SEM. p values are from Mann-Whitney U test (n = 12 based on four replicates for each, each contains about 100 brains). *p < 0.05, **p < 0.01, ***p < 0.001, ****p < 0.0001, ns indicates no significant difference.

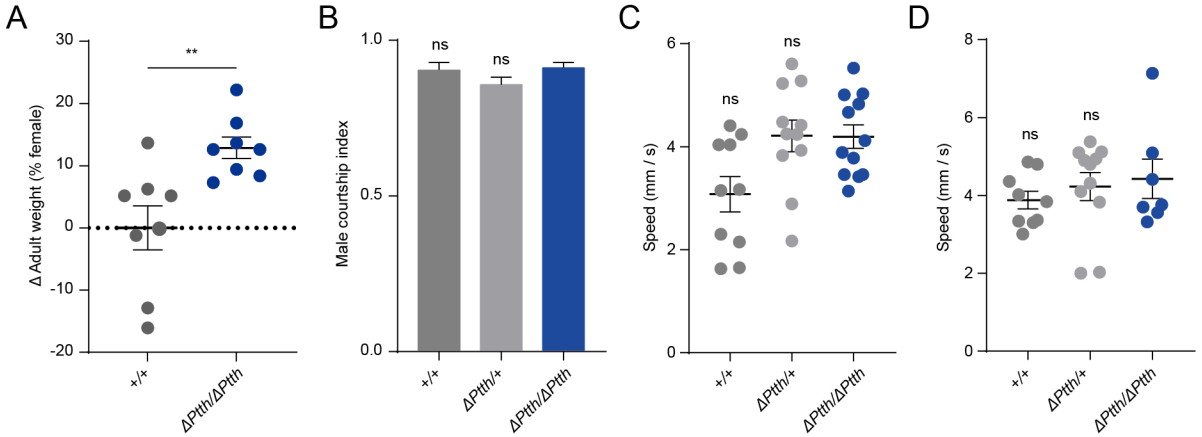

Figure 1—figure supplement 1 Weight, attractiveness and locomotion behavior of *Ptth* null mutant virgin females.

(A) The weight of 24h-old adult *ΔPtth* null mutant females was significantly higher than that of wild type females (Mann-Whitney U test, n=8 groups, 10 flies in each group). (B) Courtship index of wild-type males during the first 5 min of courtship towards a female with the indicated genotype (Kruskal-Wallis ANOVA and post hoc Mann-Whitney U tests, n = 7-9). (C-D) Mean velocity had no significant change in *ΔPtth* null mutant females on the 1st day (C) and the 6th day (D) compared with control females (Kruskal-Wallis ANOVA and post hoc Mann-Whitney U tests, n = 7-12). Error bars indicate SEM. *p < 0.05, **p < 0.01, ***p < 0.001, ****p < 0.0001, ns = not significant.

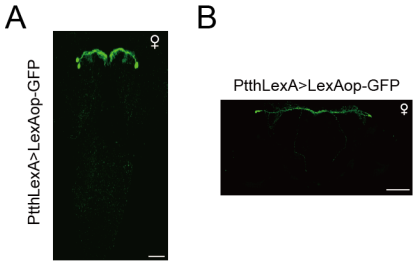

Figure 2—figure supplement 1 PG neurons expressing PTTH labeled by PtthLexA. Expression pattern of PtthLexA in the brain revealed by anti-GFP (green) in larvae brain (A) and adult brain (B). Representative of five female flies. Scale bars, 50 μm.

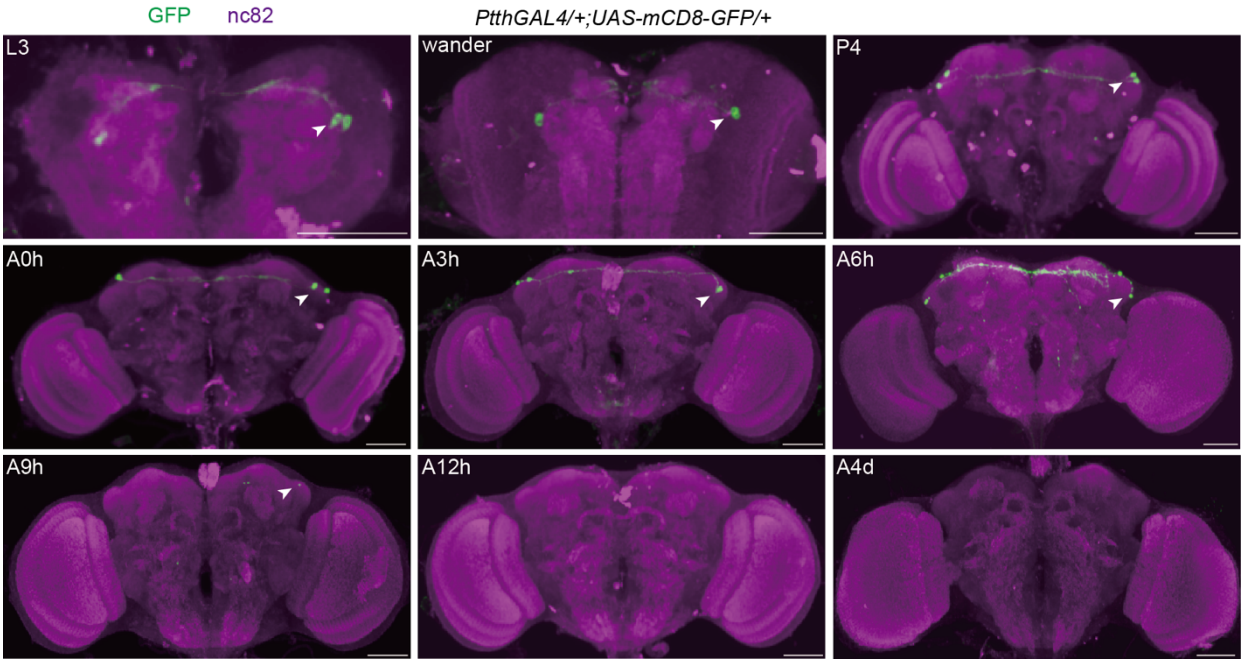

Figure 2—figure supplement 2 The anatomical pattern of PG neurons expressing PTTH at different developmental stages.

Expression pattern of PtthGAL4 in the brain revealed by anti-GFP from the 3rd larval stage to the 4th day after eclosion. Arrows show PTTH signals (green) stained with anti-GFP antibody. L3, the 3rd -instar larvae; wander, the wandering larvae; P4, the 4th day of the pupal stage; A0h, the 1st hour of the adult stage; A3h, the 3rd hour of the adult stage; A6h, the 6th hour of the adult stage; A9h, the 9th hour of the adult stage; A12h, the 12th hour of the adult stage; A4d, the 4th day of the adult stage. Representative of five female flies. Scale bars, 50 μm.

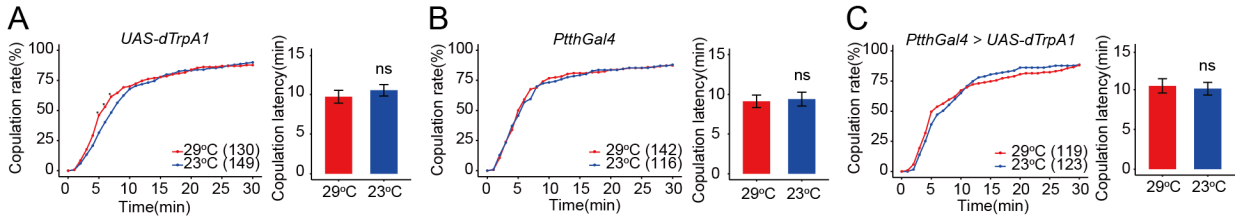

Figure 2—figure supplement 3 PG neurons expressing PTTH do not regulate virgin female copulation rate during adult stage.

PG neurons were activated during adult stage by dTrpA1 at 29°C. The female copulation rate and the latency to copulation did not change significantly. The number of female flies paired with wild-type males is displayed in parentheses. For the copulation rate, chi-square test is applied. For the latency to copulation, Mann-Whitney U test is applied. Error bars indicate SEM. *$p < 0.05$, **$p < 0.01$, ***$p < 0.001$, ****$p < 0.0001$, ns indicates no significant difference.

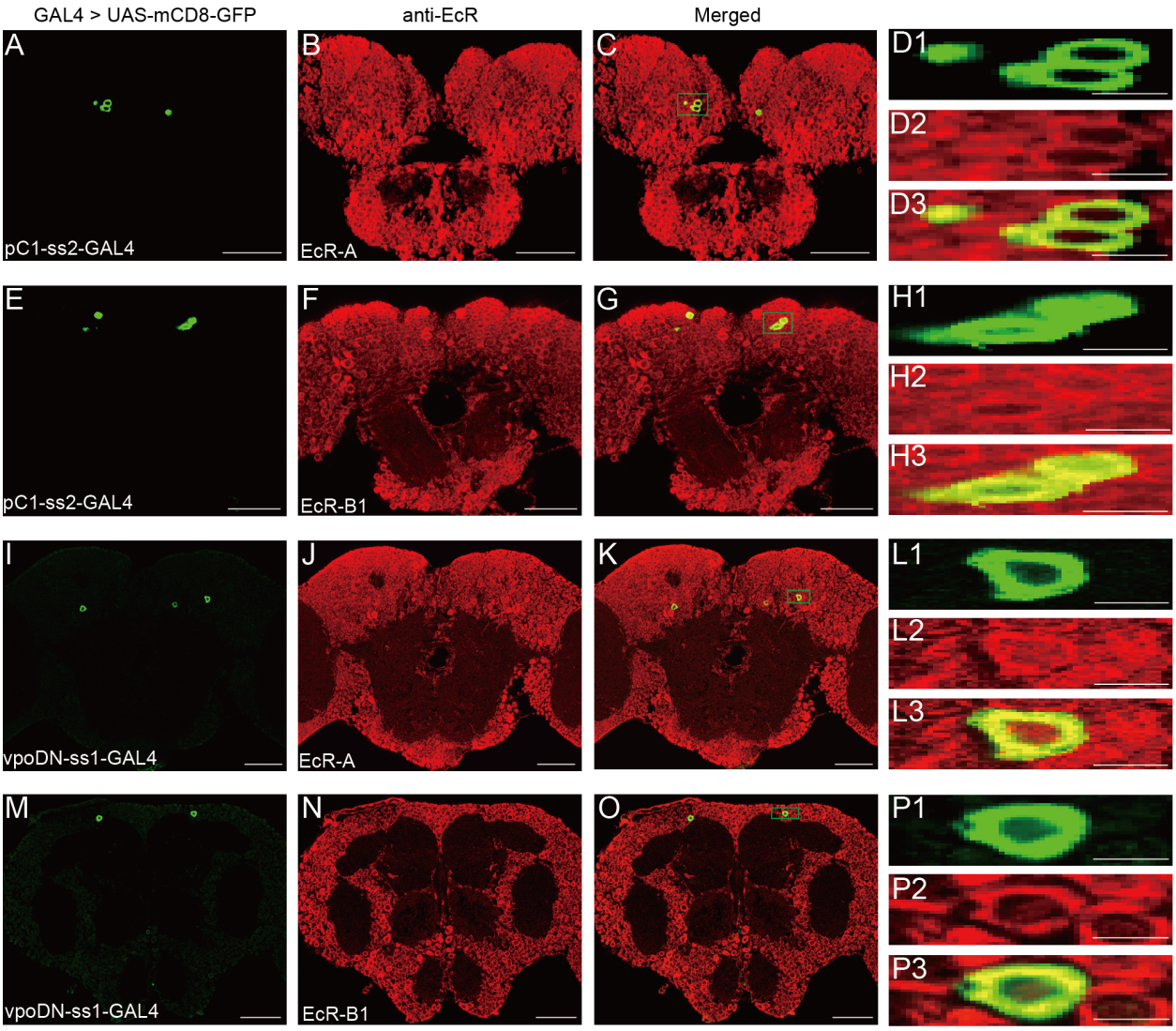

Figure 5—figure supplement 1 Expression of EcR-A and EcR-B1 in pC1 and vpoDN neurons.

(A-C) pC1 neurons were colabeled by pC1-ss2 driving UAS-mCD8-GFP (green, A) and EcR-A antibodies (red, B). Magnification of green boxed region in (C) is shown in (D1–D3). (E-G) pC1 neurons were colabeled by pC1-ss2 driving UAS-mCD8-GFP (green, E) and EcR-B1 antibodies (red, F). Magnification of green boxed region in (G) is shown in (H1–H3). (I-K) vpoDN neurons were colabeled by vpo-ss1 driving UAS-mCD8-GFP (green, I) and EcR-A antibodies (red, J). Magnification of green boxed region in (K) is shown in (L1–L3). (M-O) vpoDN neurons were colabeled by vpo-ss1 driving UAS-mCD8-GFP (green, M) and EcR-B1 antibodies (red, N). Magnification of green boxed

region in (O) is shown in (P1–P3). Scale bars for magnified regions are 5 μm, for others are 50 μm.

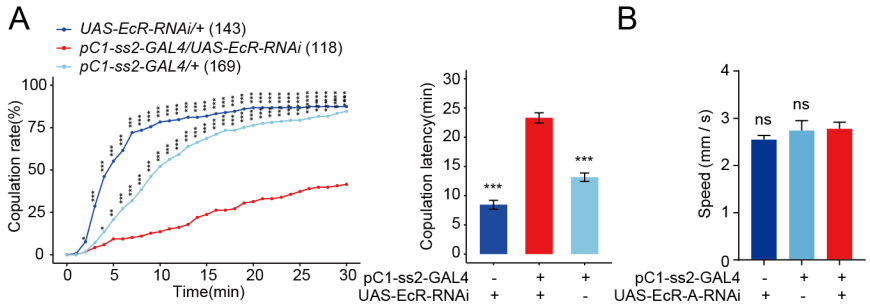

Figure 5—figure supplement 2 Reduced EcR in pC1 neurons reduces virgin female receptivity.

(A) Knock-down of EcR in pC1 neurons driven by pC1-ss2-GAL4 significantly decreased the copulation rate and increased the latency to copulation. (B) Mean velocity had no significant change when EcR-A was knocked down in pC1 neurons compared with controls (Kruskal-Wallis ANOVA and post hoc Mann-Whitney U tests, n = 8-11). The number of female flies paired with wild-type males is displayed in parentheses. For the copulation rate, chi-square test is applied. For the latency to copulation, Kruskal-Wallis ANOVA and post hoc Mann-Whitney U tests are applied. Error bars indicate SEM. *p < 0.05, **p < 0.01, ***p < 0.001, ****p < 0.0001, ns indicates no significant difference.

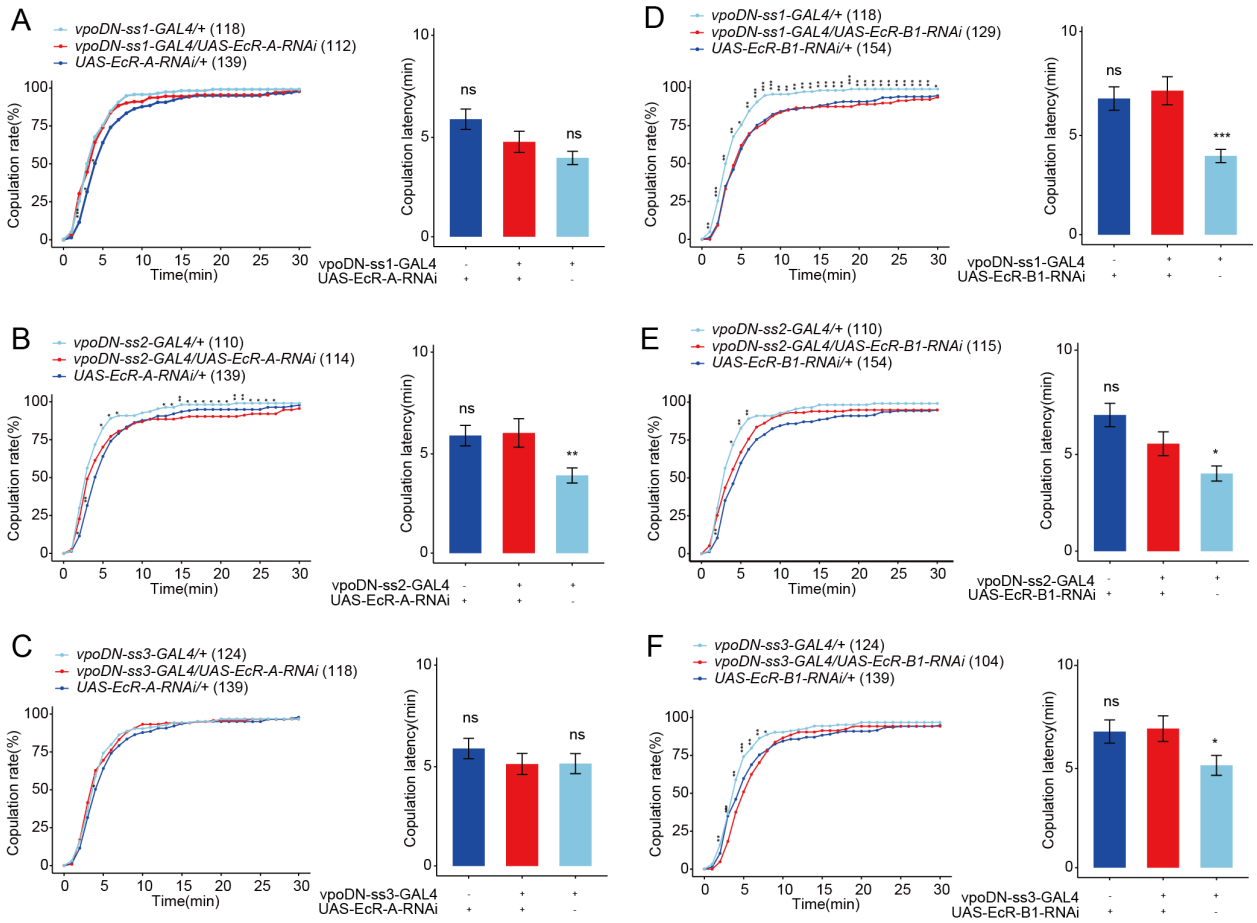

Figure 5—figure supplement 3 Reduced EcR in vpoDN neurons has no effect on virgin female receptivity.

(A-C) Knock-down of EcR-A in vpoDN neurons driven by vpoDN-ss1-GAL4, vpoDN-ss2-GAL4 and vpoDN-ss3-GAL4 had no effect on virgin female receptivity. (D-F) Knock-down of EcR-B1 in vpoDN neurons driven by vpoDN-ss1-GAL4, vpoDN-ss2-GAL4 and vpoDN-ss3-GAL4 had no effect on virgin female receptivity. The number of female flies paired with wild-type males is displayed in parentheses. For the copulation rate, chi-square test is applied. For the latency to copulation, Kruskal-Wallis ANOVA and post hoc Mann-Whitney U tests are applied. Error bars indicate SEM. *$p < 0.05$, **$p < 0.01$, ***$p < 0.001$, ****$p < 0.0001$, ns indicates no significant difference.

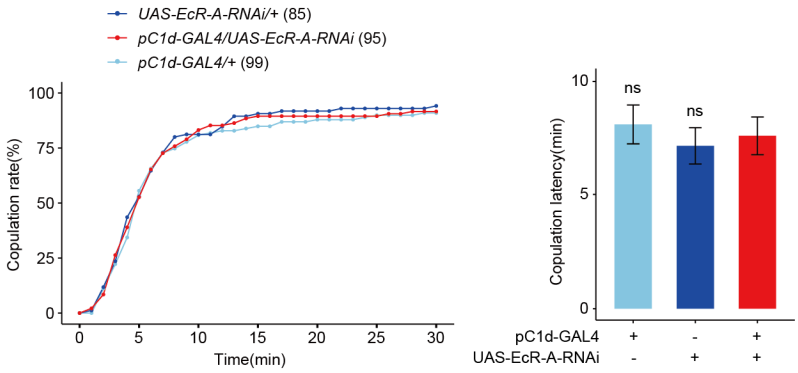

Figure 5—figure supplement 4 Reduced EcR-A in pC1d neurons has no effect on virgin female receptivity.

(A) Knock-down of EcR-A in pC1d neurons had no effect on virgin female copulation rate and latency to copulation. The number of female flies paired with wild-type males is displayed in parentheses. For the copulation rate, chi-square test is applied. For the latency to copulation, Kruskal-Wallis ANOVA and post hoc Mann-Whitney U tests are applied. Error bars indicate SEM, *p < 0.05, **p < 0.01, ***p < 0.001, ****p < 0.0001, ns indicates no significant difference.

1412 **Supplementary File 1.** The primers used for the verification of *ΔPtth* null mutant flies
1413 and for the real-time quantitative PCR of dopamine beta-monooxygenase (DBM).
1414
1415 **Supplementary File 2.** The differently expressed genes in whole brains between flies
1416 having reduced EcR-A expression in pC1 neurons and the control flies.
1417
1418 **Supplementary File 3.** The raw data of transcriptomes in whole brains when EcR-A
1419 was knocked down in pC1 neurons or not.
1420
1421 **Figure 1—Source Data 1.** Photo of nucleic acid electrophoresis and copulation time.
1422
1423 **Figure 2—Source Data 1.** Copulation time.
1424
1425 **Figure 3—Source Data 1.** Copulation time and walking speed.
1426
1427 **Figure 4—Source Data 1.** Copulation time.
1428
1429 **Figure 5—Source Data 1.** Copulation time, courtship index, number of eggs, number of
1430 vaginal plate opening (VPO), and number of ovipositor extrusion (OE).
1431
1432 **Figure 6—Source Data 1.** Fluorescence intensity, cell number and calcium activity.
1433
1434 **Figure 7—Source Data 1.** Relative mRNA level.
1435
1436 **Figure 1—figure supplement 1—Source Data 1.** Body weight, courtship index and
1437 walking speed.
1438
1439 **Figure 2—figure supplement 3—Source Data 1.** Copulation time.
1440
1441 **Figure 5—figure supplement 2—Source Data 1.** Copulation time and walking speed.
1442

1443 **Figure 5—figure supplement 3—Source Data 1.** Copulation time.

1444

1445 **Figure 5—figure supplement 4—Source Data 1.** Copulation time.

1446

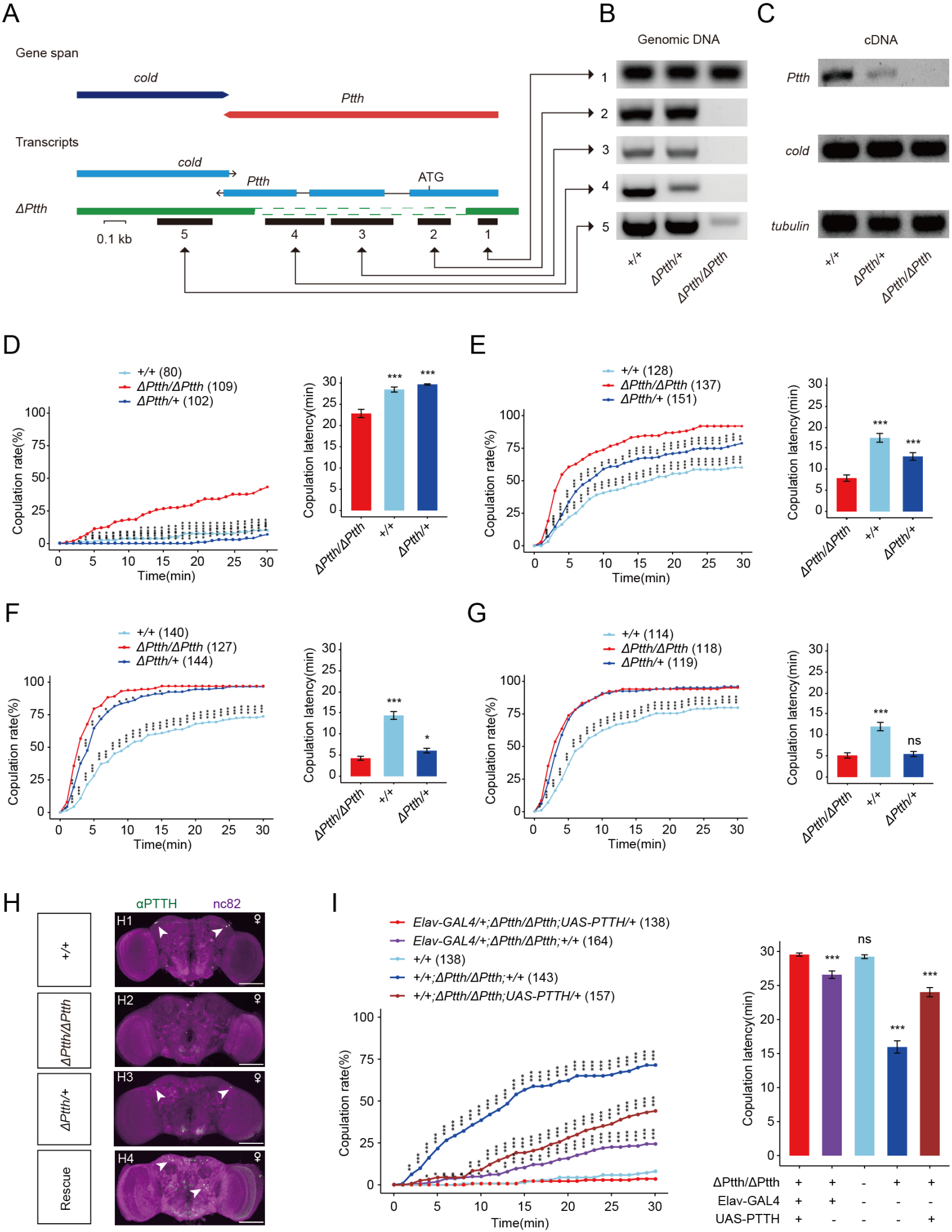
A
Gene span
cold
Ptth
Transcripts
cold
Ptth
ATG
ΔPtth
0.1 kb
5
4
3
2
1
B
Genomic DNA
1
2
3
4
5
+/+
ΔPtth/+
ΔPtth/ΔPtth
C
cDNA
Ptth
cold
tubulin
+/+
ΔPtth/+
ΔPtth/ΔPtth
D
+/+ (80)
ΔPtth/ΔPtth (109)
ΔPtth/+ (102)
Copulation rate(%)
Time(min)
Copulation latency(min)
ΔPtth/ΔPtth
+/+
ΔPtth/+
E
+/+ (128)
ΔPtth/ΔPtth (137)
ΔPtth/+ (151)
Copulation rate(%)
Time(min)
Copulation latency(min)
ΔPtth/ΔPtth
+/+
ΔPtth/+
F
+/+ (140)
ΔPtth/ΔPtth (127)
ΔPtth/+ (144)
Copulation rate(%)
Time(min)
Copulation latency(min)
ΔPtth/ΔPtth
+/+
ΔPtth/+
G
+/+ (114)
ΔPtth/ΔPtth (118)
ΔPtth/+ (119)
Copulation rate(%)
Time(min)
Copulation latency(min)
ns
ΔPtth/ΔPtth
+/+
ΔPtth/+
H
αPTTH
nc82
+/+
ΔPtth/ΔPtth
ΔPtth/+
Rescue
H1
H2
H3
H4
I
Elav-GAL4/+;ΔPtth/ΔPtth;UAS-PTTH/+ (138)
Elav-GAL4/+;ΔPtth/ΔPtth;+/+ (164)
+/+ (138)
+/+;ΔPtth/ΔPtth;+/+ (143)
+/+;ΔPtth/ΔPtth;UAS-PTTH/+ (157)
Copulation rate(%)
Time(min)
Copulation latency(min)
ns
ΔPtth/ΔPtth + + - + +
Elav-GAL4 + + - - -
UAS-PTTH + - - - +

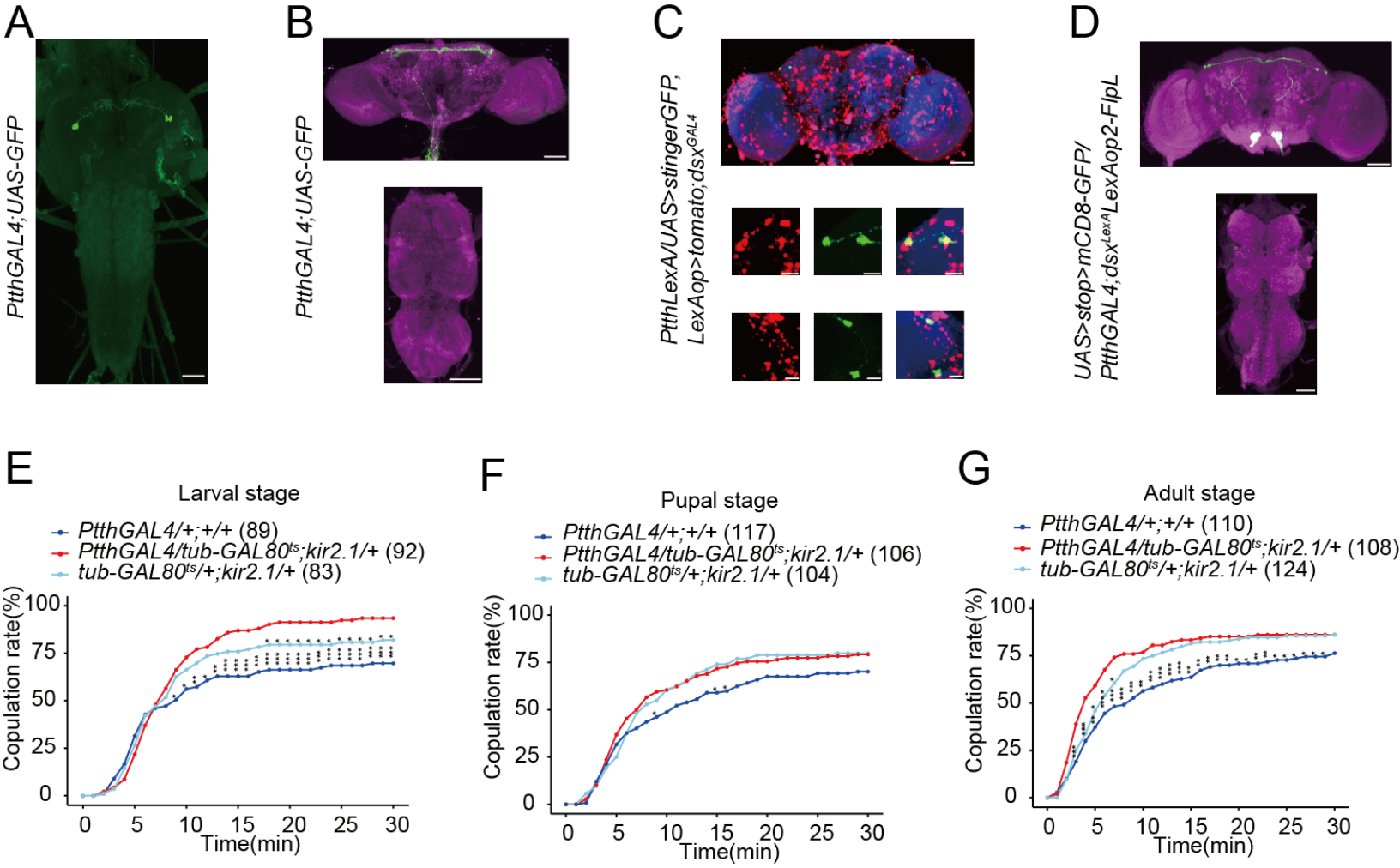
A
PtthGAL4;UAS-GFP
B
PtthGAL4;UAS-GFP
C
PtthLexA/UAS>stingerGFP, LexAop>tomato;dsxGAL4
D
UAS>stop>mCD8-GFP/ PtthGAL4;dsxLexALexAop2-FlpL
E
Larval stage
PtthGAL4/+;+/+ (89)
PtthGAL4/tub-GAL80ts;kir2.1/+ (92)
tub-GAL80ts/+;kir2.1/+ (83)
Copulation rate(%)
Time(min)
F
Pupal stage
PtthGAL4/+;+/+ (117)
PtthGAL4/tub-GAL80ts;kir2.1/+ (106)
tub-GAL80ts/+;kir2.1/+ (104)
Copulation rate(%)
Time(min)
G
Adult stage
PtthGAL4/+;+/+ (110)
PtthGAL4/tub-GAL80ts;kir2.1/+ (108)
tub-GAL80ts/+;kir2.1/+ (124)
Copulation rate(%)
Time(min)

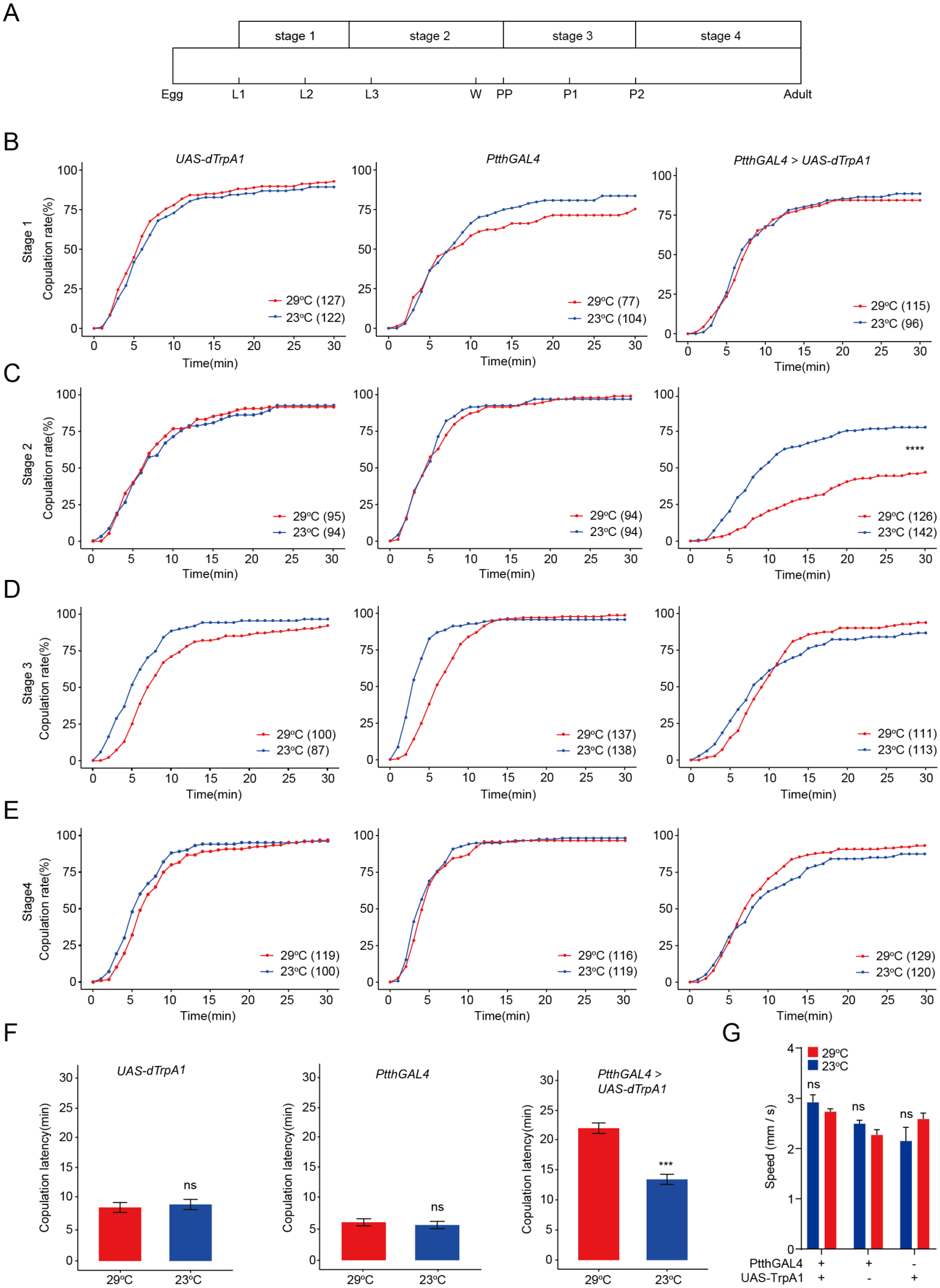
A
stage 1
stage 2
stage 3
stage 4
Egg
L1
L2
L3
W
PP
P1
P2
Adult
B
UAS-dTrpA1
PtthGAL4
PtthGAL4 > UAS-dTrpA1
Stage 1
Copulation rate(%)
Time(min)
29ºC (127)
23ºC (122)
29ºC (77)
23ºC (104)
29ºC (115)
23ºC (96)
C
Stage 2
29ºC (95)
23ºC (94)
29ºC (94)
23ºC (94)
****
29ºC (126)
23ºC (142)
D
Stage 3
29ºC (100)
23ºC (87)
29ºC (137)
23ºC (138)
29ºC (111)
23ºC (113)
E
Stage4
29ºC (119)
23ºC (100)
29ºC (116)
23ºC (119)
29ºC (129)
23ºC (120)
F
UAS-dTrpA1
PtthGAL4
PtthGAL4 > UAS-dTrpA1
Copulation latency(min)
ns
***
29ºC
23ºC
G
29ºC
23ºC
Speed (mm / s)
PtthGAL4
UAS-TrpA1

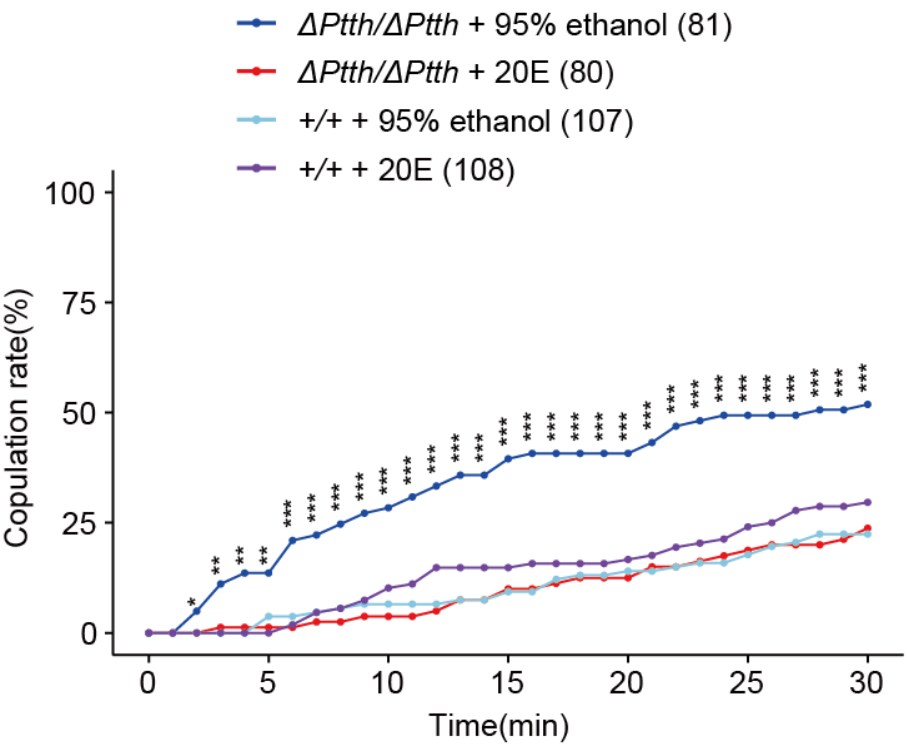
ΔPtth/ΔPtth + 95% ethanol (81)
ΔPtth/ΔPtth + 20E (80)
+/+ + 95% ethanol (107)
+/+ + 20E (108)
Copulation rate(%)
Time(min)

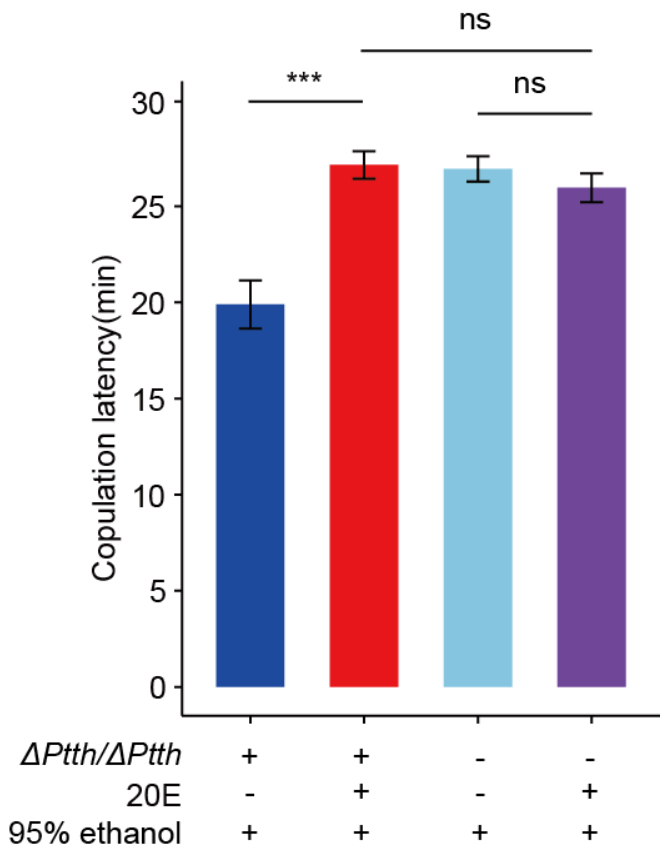
ns
***
ns
Copulation latency(min)
ΔPtth/ΔPtth + + - -
20E - + - +
95% ethanol + + + +

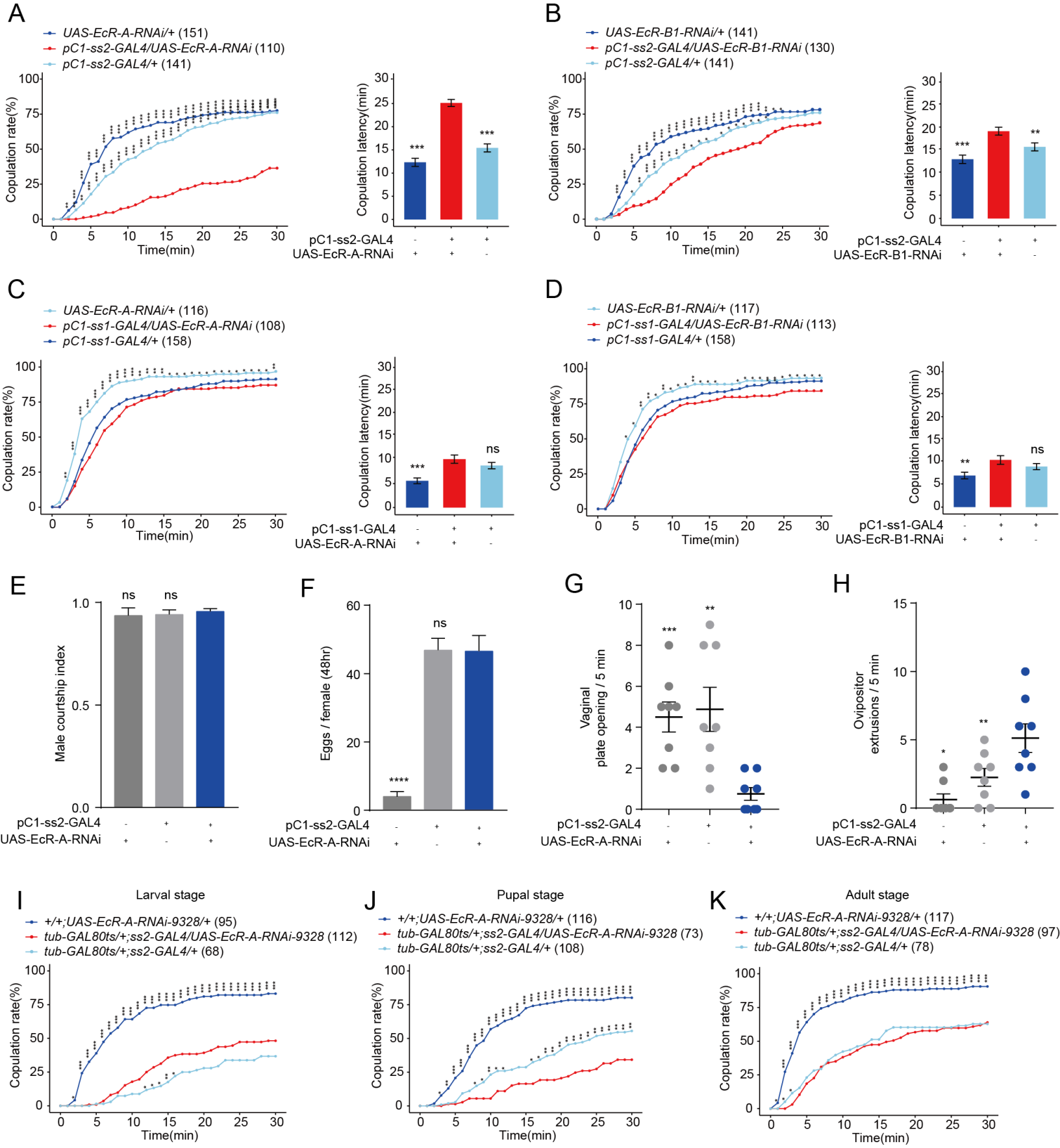
A
UAS-EcR-A-RNAi/+ (151)
pC1-ss2-GAL4/UAS-EcR-A-RNAi (110)
pC1-ss2-GAL4/+ (141)
Copulation rate(%)
Time(min)
Copulation latency(min)
pC1-ss2-GAL4
UAS-EcR-A-RNAi
B
UAS-EcR-B1-RNAi/+ (141)
pC1-ss2-GAL4/UAS-EcR-B1-RNAi (130)
pC1-ss2-GAL4/+ (141)
Copulation rate(%)
Time(min)
Copulation latency(min)
pC1-ss2-GAL4
UAS-EcR-B1-RNAi
C
UAS-EcR-A-RNAi/+ (116)
pC1-ss1-GAL4/UAS-EcR-A-RNAi (108)
pC1-ss1-GAL4/+ (158)
Copulation rate(%)
Time(min)
Copulation latency(min)
pC1-ss1-GAL4
UAS-EcR-A-RNAi
D
UAS-EcR-B1-RNAi/+ (117)
pC1-ss1-GAL4/UAS-EcR-B1-RNAi (113)
pC1-ss1-GAL4/+ (158)
Copulation rate(%)
Time(min)
Copulation latency(min)
pC1-ss1-GAL4
UAS-EcR-B1-RNAi
E
Male courtship index
pC1-ss2-GAL4
UAS-EcR-A-RNAi
F
Eggs / female (48hr)
pC1-ss2-GAL4
UAS-EcR-A-RNAi
G
Vaginal plate opening / 5 min
pC1-ss2-GAL4
UAS-EcR-A-RNAi
H
Ovipositor extrusions / 5 min
pC1-ss2-GAL4
UAS-EcR-A-RNAi
I
Larval stage
+/+;UAS-EcR-A-RNAi-9328/+ (95)
tub-GAL80ts/+;ss2-GAL4/UAS-EcR-A-RNAi-9328 (112)
tub-GAL80ts/+;ss2-GAL4/+ (68)
Copulation rate(%)
Time(min)
J
Pupal stage
+/+;UAS-EcR-A-RNAi-9328/+ (116)
tub-GAL80ts/+;ss2-GAL4/UAS-EcR-A-RNAi-9328 (73)
tub-GAL80ts/+;ss2-GAL4/+ (108)
Copulation rate(%)
Time(min)
K
Adult stage
+/+;UAS-EcR-A-RNAi-9328/+ (117)
tub-GAL80ts/+;ss2-GAL4/UAS-EcR-A-RNAi-9328 (97)
tub-GAL80ts/+;ss2-GAL4/+ (78)
Copulation rate(%)
Time(min)

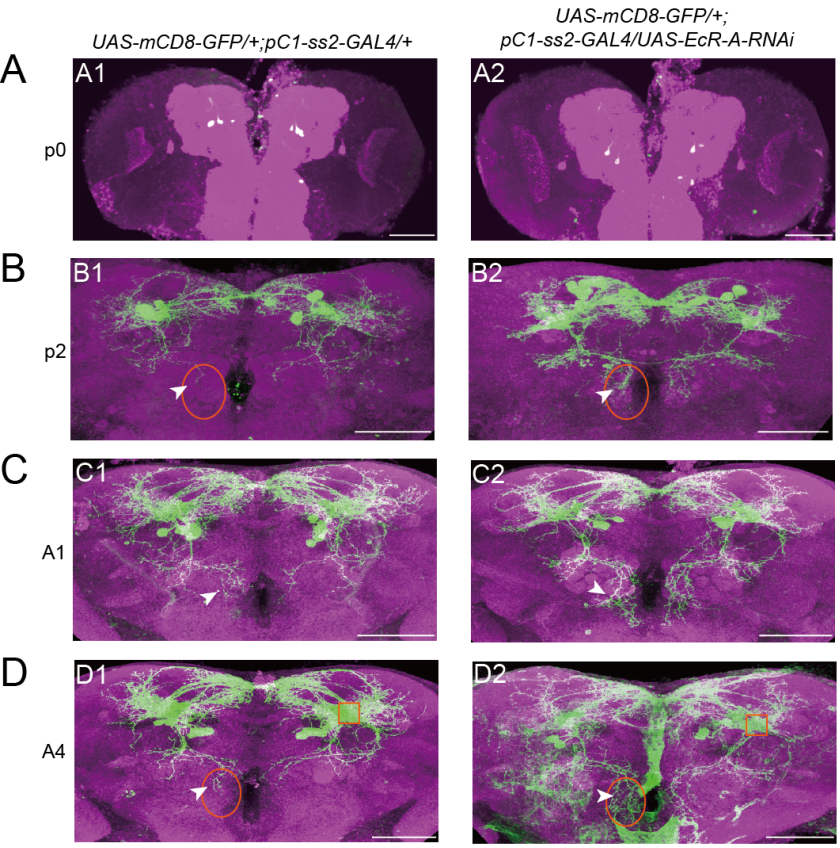
UAS-mCD8-GFP/+;pC1-ss2-GAL4/+
UAS-mCD8-GFP/+;
pC1-ss2-GAL4/UAS-EcR-A-RNAi
A
A1
A2
p0
B
B1
B2
p2
C
C1
C2
A1
D
D1
D2
A4

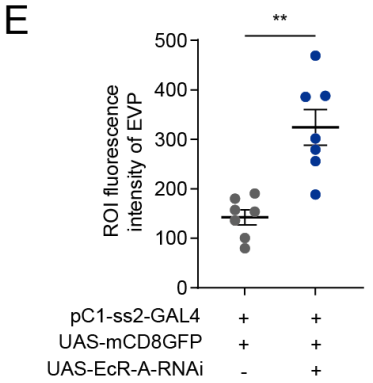
E
**
ROI fluorescence intensity of EVP
500
400
300
200
100
0
pC1-ss2-GAL4 + +
UAS-mCD8GFP + +
UAS-EcR-A-RNAi - +

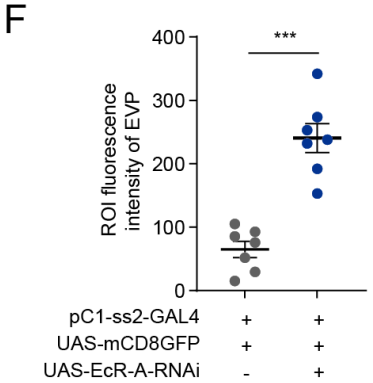
F
***
ROI fluorescence intensity of EVP
400
300
200
100
0
pC1-ss2-GAL4 + +
UAS-mCD8GFP + +
UAS-EcR-A-RNAi - +

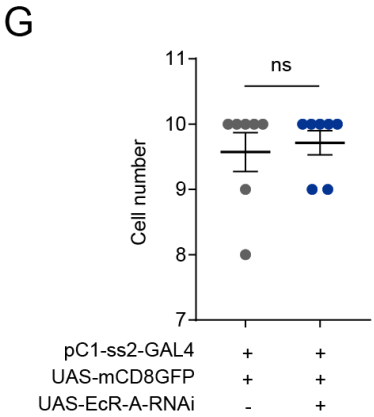
G
ns
Cell number
11
10
9
8
7
pC1-ss2-GAL4 + +
UAS-mCD8GFP + +
UAS-EcR-A-RNAi - +

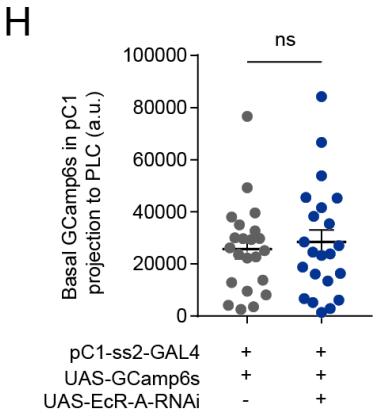
H
ns
Basal GCamp6s in pC1 projection to PLC (a.u.)
100000
80000
60000
40000
20000
0
pC1-ss2-GAL4 + +
UAS-GCamp6s + +
UAS-EcR-A-RNAi - +

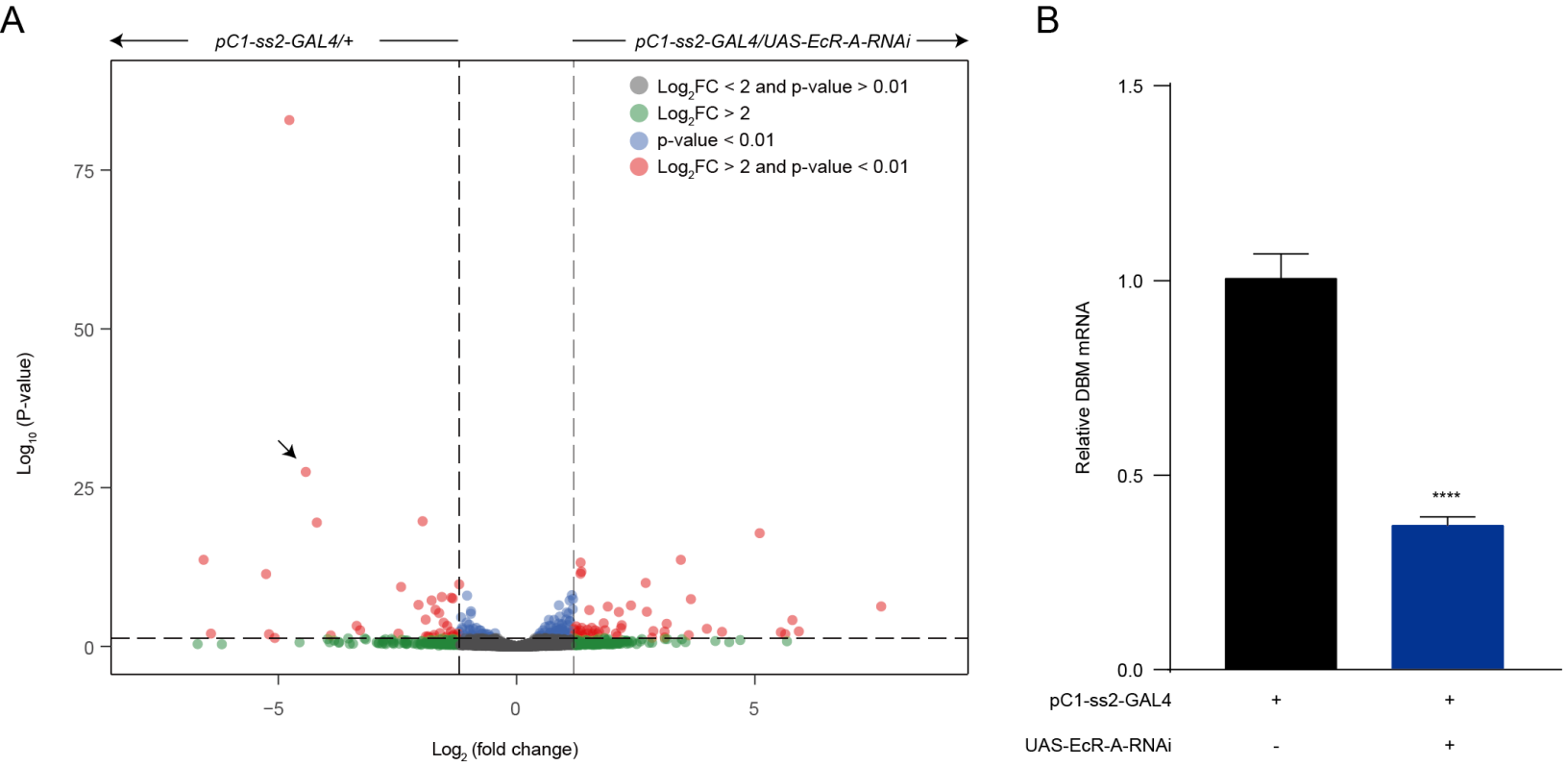
A
pC1-ss2-GAL4/+
pC1-ss2-GAL4/UAS-EcR-A-RNAi
Log2FC < 2 and p-value > 0.01
Log2FC > 2
p-value < 0.01
Log2FC > 2 and p-value < 0.01
Log10 (P-value)
75
50
25
0
−5
0
5
Log2 (fold change)
B
Relative DBM mRNA
1.5
1.0
0.5
0.0
****
pC1-ss2-GAL4
+
+
UAS-EcR-A-RNAi
-
+

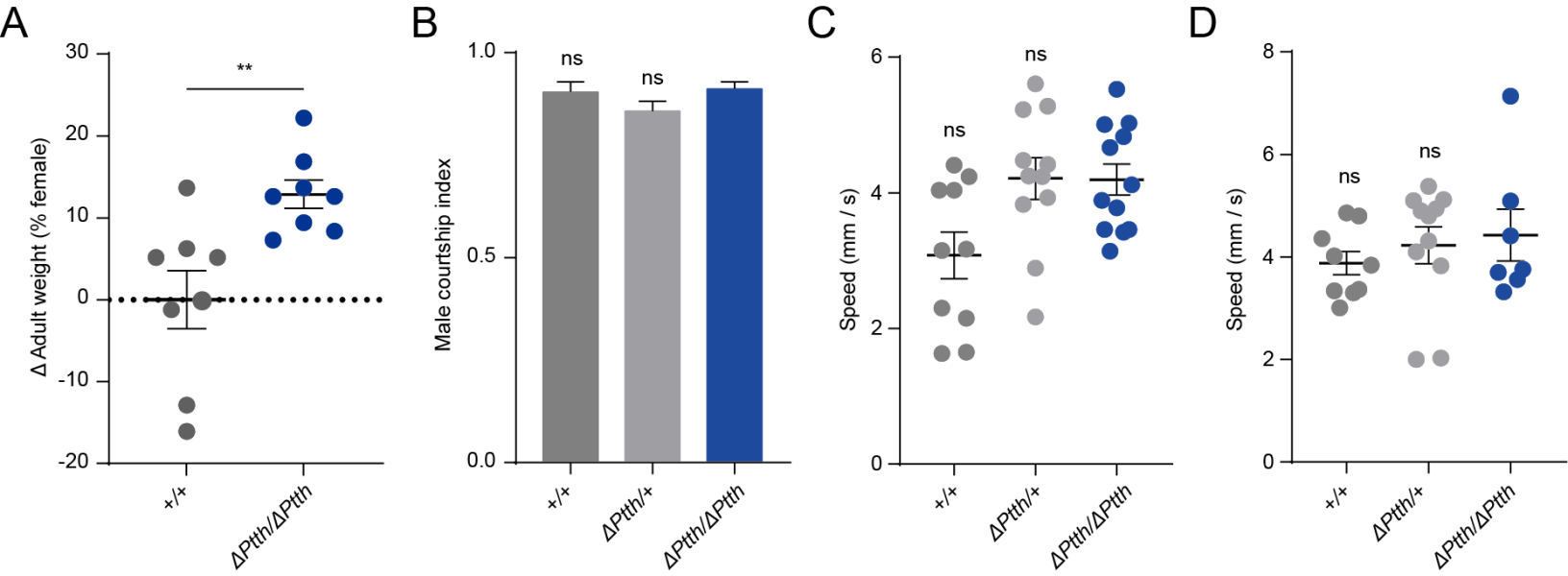
A
B
C
D
Δ Adult weight (% female)
30
20
10
0
-10
-20
**
+/+
ΔPtth/ΔPtth
Male courtship index
1.0
0.5
0.0
ns
ns
+/+
ΔPtth/+
ΔPtth/ΔPtth
Speed (mm / s)
6
4
2
0
ns
ns
+/+
ΔPtth/+
ΔPtth/ΔPtth
Speed (mm / s)
8
6
4
2
0
ns
ns
+/+
ΔPtth/+
ΔPtth/ΔPtth

A

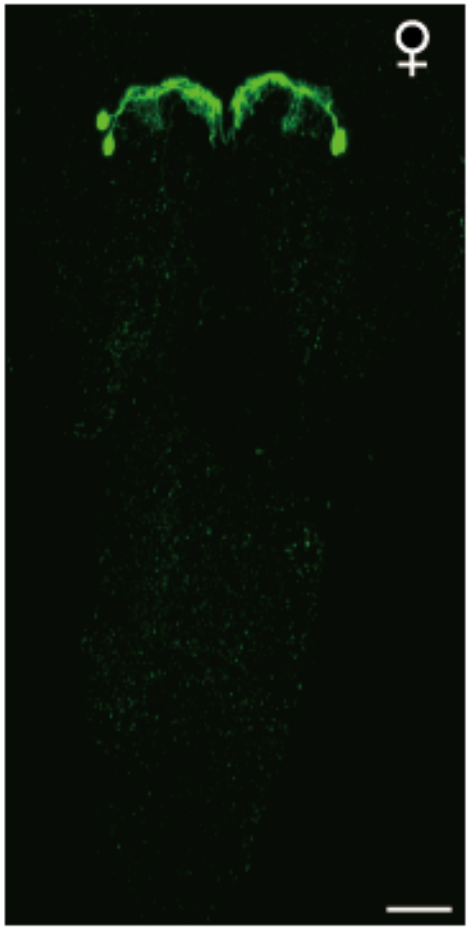

PtthLexA>LexAop-GFP

B

PtthLexA>LexAop-GFP

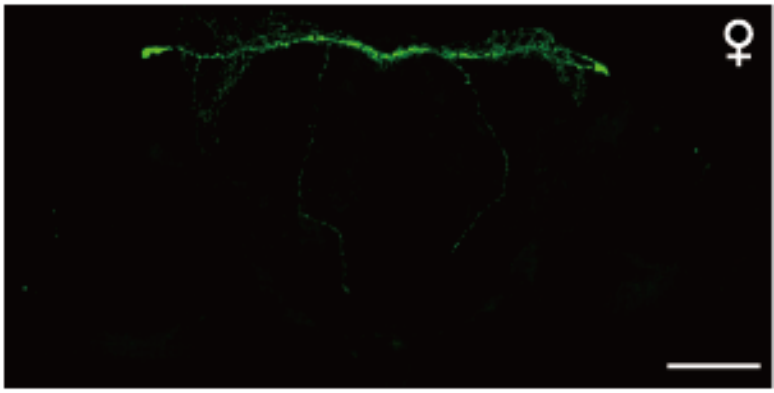

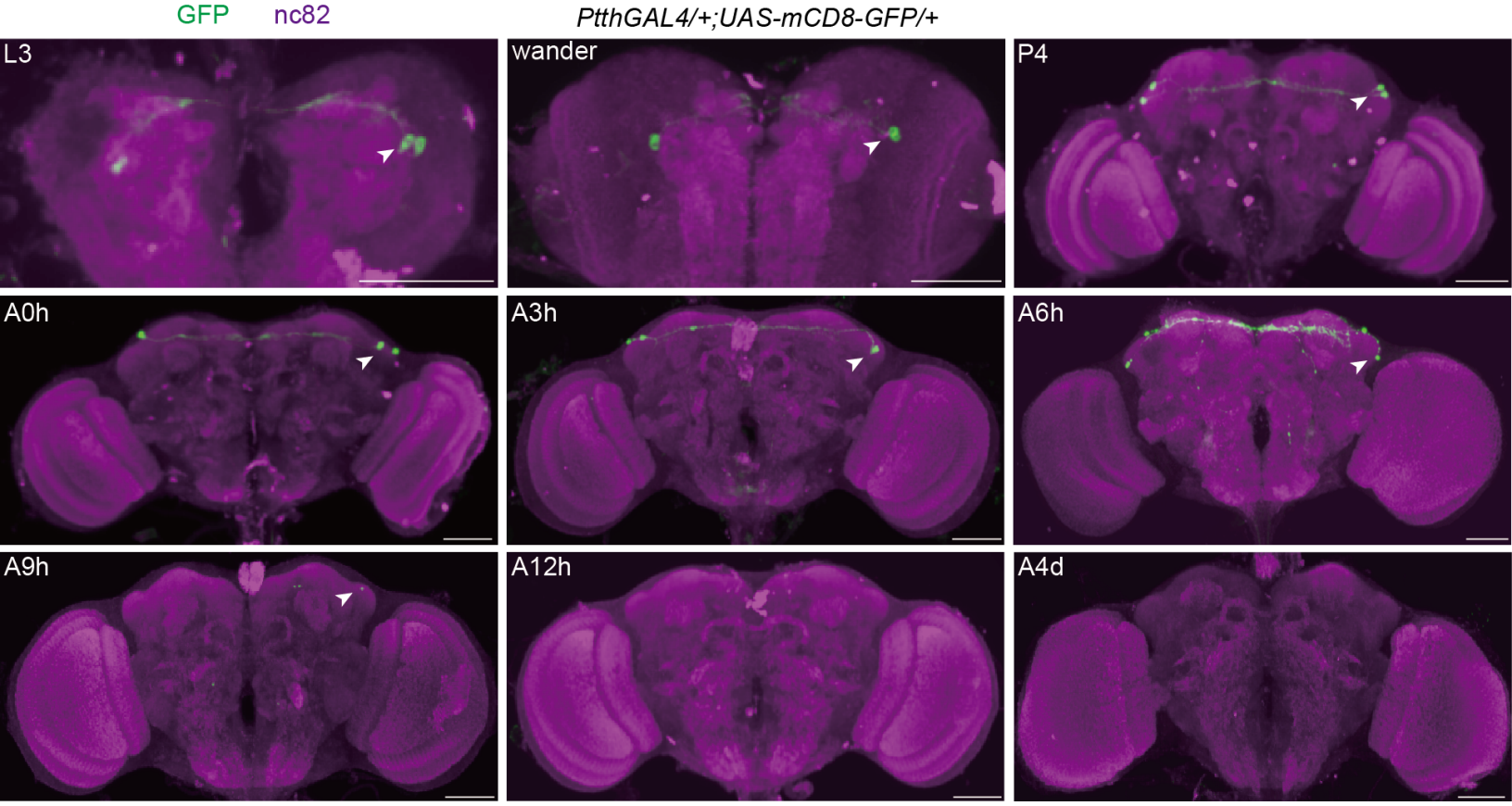
GFP
nc82
PtthGAL4/+;UAS-mCD8-GFP/+
L3
wander
P4
A0h
A3h
A6h
A9h
A12h
A4d

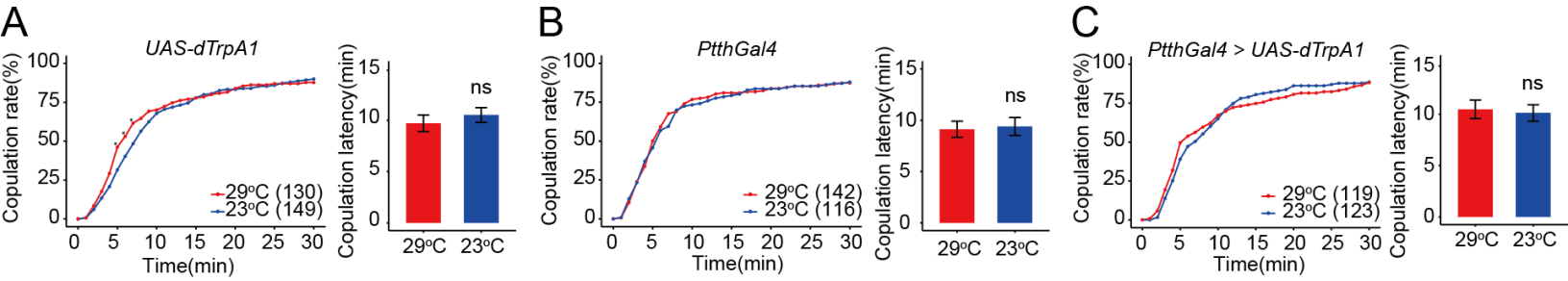
A
UAS-dTrpA1
Copulation rate(%)
100
75
50
25
0
29ºC (130)
23ºC (149)
0 5 10 15 20 25 30
Time(min)
Copulation latency(min)
15
10
5
0
ns
29ºC 23ºC
B
PtthGal4
Copulation rate(%)
100
75
50
25
0
29ºC (142)
23ºC (116)
0 5 10 15 20 25 30
Time(min)
Copulation latency(min)
15
10
5
0
ns
29ºC 23ºC
C
PtthGal4 > UAS-dTrpA1
Copulation rate(%)
100
75
50
25
0
29ºC (119)
23ºC (123)
0 5 10 15 20 25 30
Time(min)
Copulation latency(min)
15
10
5
0
ns
29ºC 23ºC

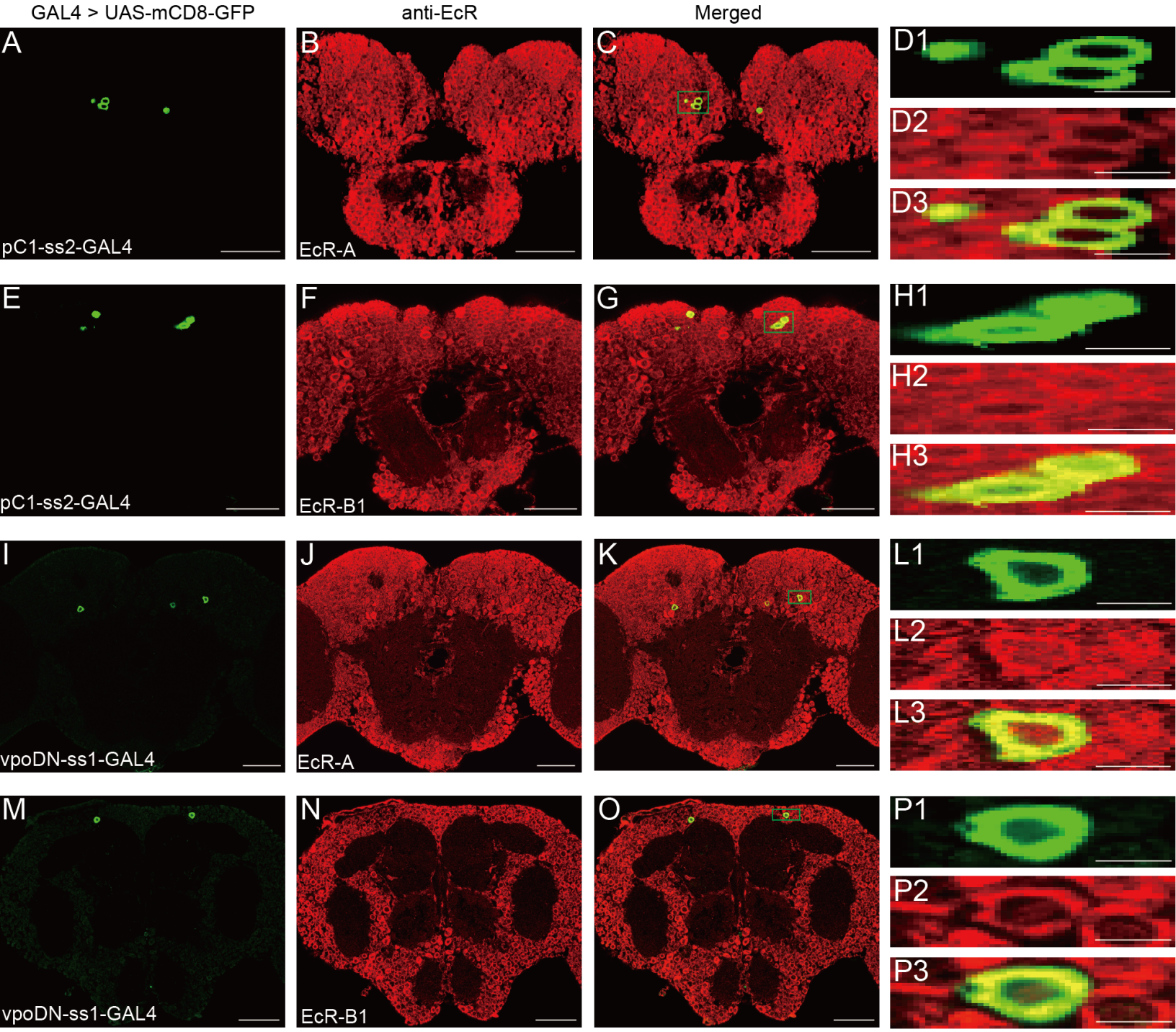
GAL4 > UAS-mCD8-GFP
anti-EcR
Merged
A
B
C
D1
D2
D3
pC1-ss2-GAL4
EcR-A
E
F
G
H1
H2
H3
pC1-ss2-GAL4
EcR-B1
I
J
K
L1
L2
L3
vpoDN-ss1-GAL4
EcR-A
M
N
O
P1
P2
P3
vpoDN-ss1-GAL4
EcR-B1

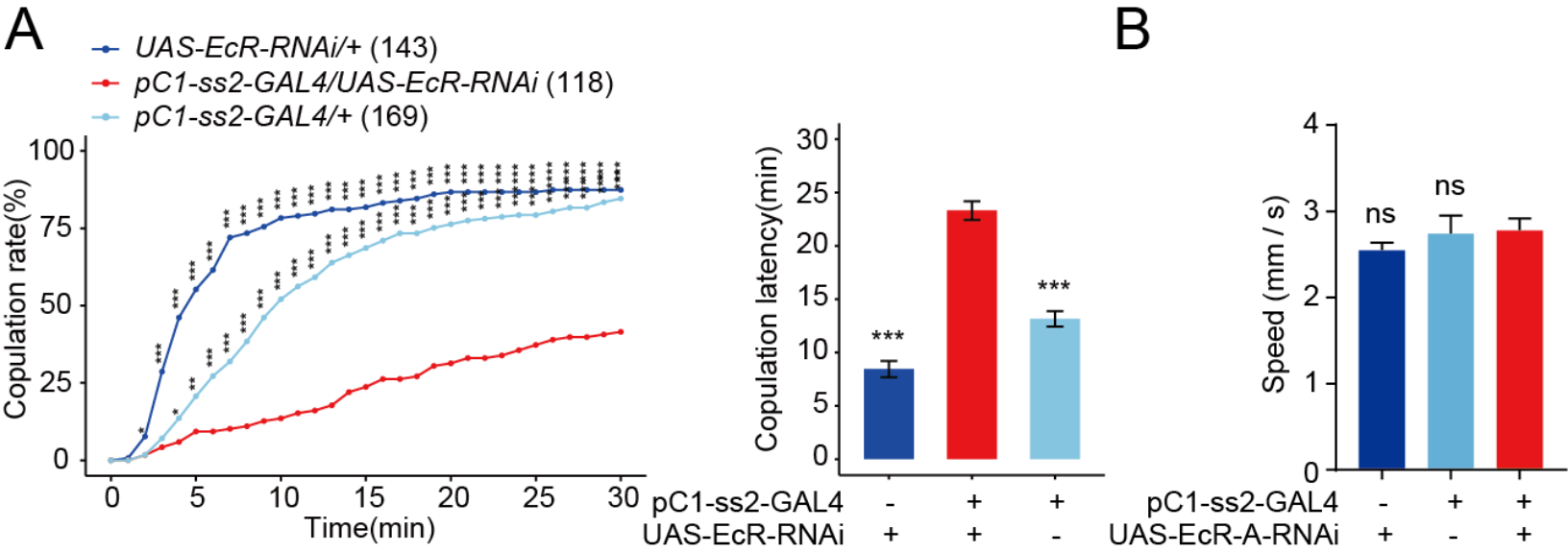
A
UAS-EcR-RNAi/+ (143)
pC1-ss2-GAL4/UAS-EcR-RNAi (118)
pC1-ss2-GAL4/+ (169)
Copulation rate(%)
Time(min)
Copulation latency(min)
pC1-ss2-GAL4 - + +
UAS-EcR-RNAi + + -
B
Speed (mm / s)
ns
ns
pC1-ss2-GAL4 - + +
UAS-EcR-A-RNAi + - +

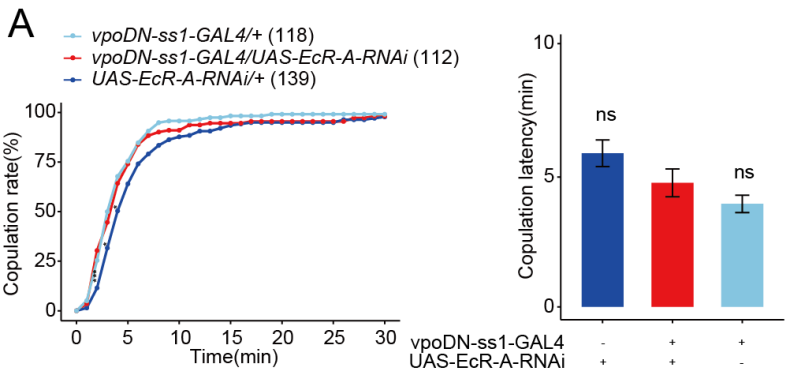
A
vpoDN-ss1-GAL4/+ (118)
vpoDN-ss1-GAL4/UAS-EcR-A-RNAi (112)
UAS-EcR-A-RNAi/+ (139)
Copulation rate(%)
Time(min)
Copulation latency(min)
ns
ns
vpoDN-ss1-GAL4
UAS-EcR-A-RNAi

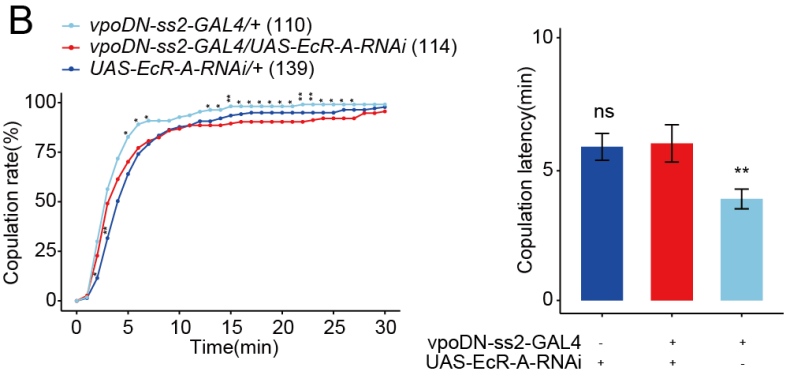
B
vpoDN-ss2-GAL4/+ (110)
vpoDN-ss2-GAL4/UAS-EcR-A-RNAi (114)
UAS-EcR-A-RNAi/+ (139)
Copulation rate(%)
Time(min)
Copulation latency(min)
ns
**
vpoDN-ss2-GAL4
UAS-EcR-A-RNAi

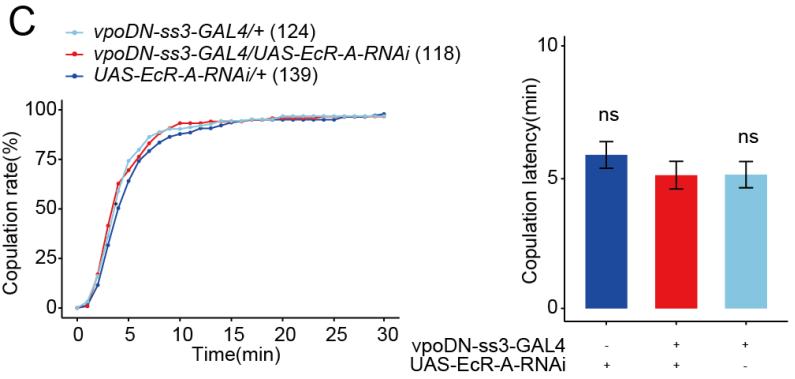
C
vpoDN-ss3-GAL4/+ (124)
vpoDN-ss3-GAL4/UAS-EcR-A-RNAi (118)
UAS-EcR-A-RNAi/+ (139)
Copulation rate(%)
Time(min)
Copulation latency(min)
ns
ns
vpoDN-ss3-GAL4
UAS-EcR-A-RNAi

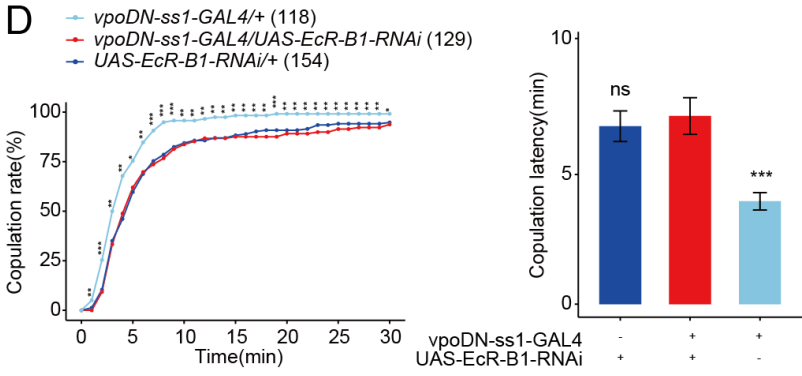
D
vpoDN-ss1-GAL4/+ (118)
vpoDN-ss1-GAL4/UAS-EcR-B1-RNAi (129)
UAS-EcR-B1-RNAi/+ (154)
Copulation rate(%)
Time(min)
Copulation latency(min)
ns
***
vpoDN-ss1-GAL4
UAS-EcR-B1-RNAi

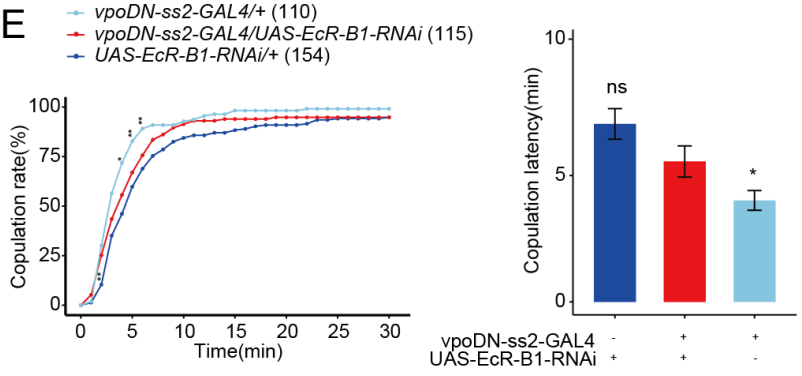
E
vpoDN-ss2-GAL4/+ (110)
vpoDN-ss2-GAL4/UAS-EcR-B1-RNAi (115)
UAS-EcR-B1-RNAi/+ (154)
Copulation rate(%)
Time(min)
Copulation latency(min)
ns
*
vpoDN-ss2-GAL4
UAS-EcR-B1-RNAi

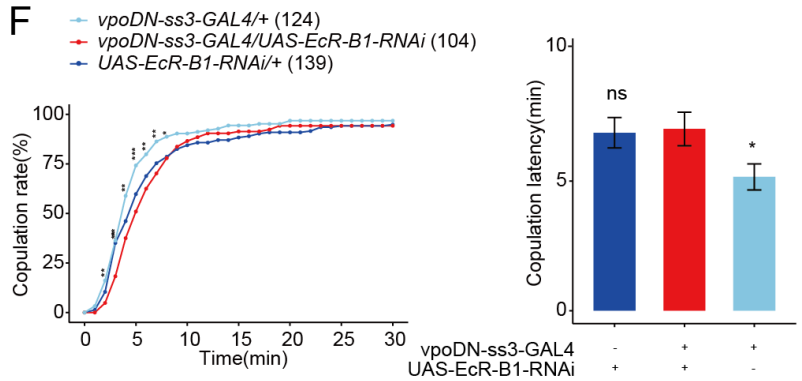
F
vpoDN-ss3-GAL4/+ (124)
vpoDN-ss3-GAL4/UAS-EcR-B1-RNAi (104)
UAS-EcR-B1-RNAi/+ (139)
Copulation rate(%)
Time(min)
Copulation latency(min)
ns
*
vpoDN-ss3-GAL4
UAS-EcR-B1-RNAi

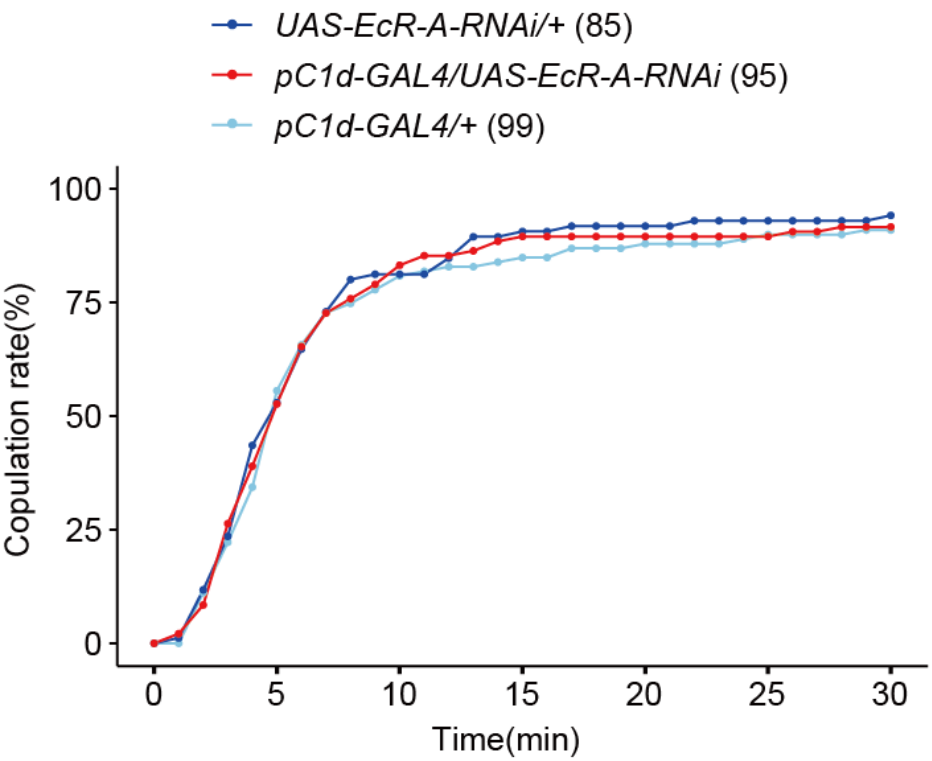
UAS-EcR-A-RNAi/+ (85)
pC1d-GAL4/UAS-EcR-A-RNAi (95)
pC1d-GAL4/+ (99)
Copulation rate(%)
100
75
50
25
0
0
5
10
15
20
25
30
Time(min)

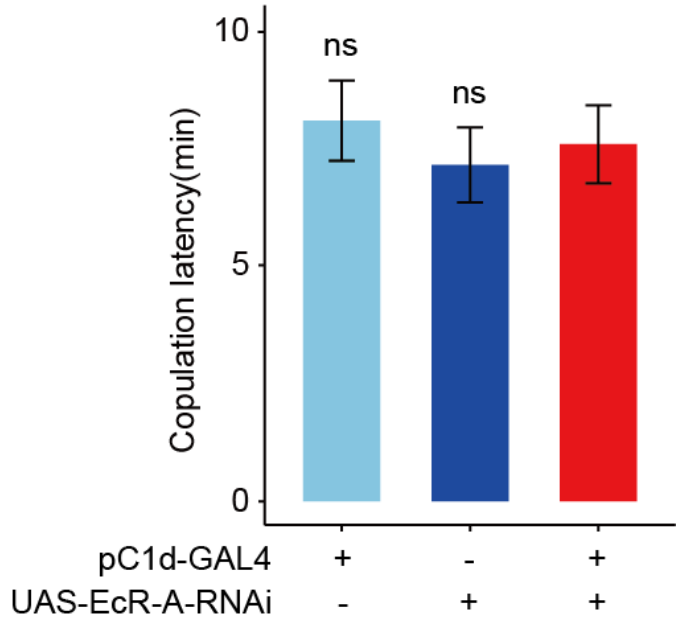
Copulation latency(min)
10
5
0
ns
ns
pC1d-GAL4 + - +
UAS-EcR-A-RNAi - + +